



# Secondary production at the Barents Sea polar front in summer: contribution of different size classes of mesozooplankton

Christine Gawinski<sup>1,\*</sup>, Sünne Linnéa Basedow<sup>1</sup>, Arild Sundfjord<sup>2</sup>, Camilla Svensen<sup>1</sup>

<sup>1</sup>Department of Arctic and Marine Biology, Faculty of Biosciences, Fisheries and Economics, UiT The Arctic University of Norway, 9019 Tromsø, Norway

<sup>2</sup>Norwegian Polar Institute, 9296 Tromsø, Norway

**ABSTRACT:** The Barents Sea polar front is characterized by high primary production following the retreat of the ice edge during spring. However, secondary production estimates of mesozooplankton across the front are scarce, despite being essential for understanding energy flow through the food web. We investigated mesozooplankton community composition and production across the Barents Sea polar front ( $75^{\circ}$ – $78^{\circ}$  N) in June, covering both Atlantic and Arctic water masses with high spatial and taxonomic resolution. We highlight the contribution of small and large groups of mesozooplankton and estimate secondary production by comparing and evaluating 4 commonly used growth rate models. The zooplankton community composition and size distribution changed across the polar front. In the Atlantic region, Rotifera, Chaetognatha and Appendicularia were common, while copepods and their nauplii contributed most across the polar front and in Arctic water masses. Mesozooplankton secondary production took place mainly in the surface and was highest south of the front, declining towards Arctic waters. Considering production by copepods alone, highest values were found in the northern sector of the polar front and in the Arctic region. Young developmental stages (CI–CIV) of *Calanus* spp. and small-sized taxa contributed most to copepod production in Atlantic waters, while calanoid copepod nauplii contributed considerably to copepod production in Arctic waters. We emphasize that the production estimates were strongly influenced by the growth rate model and conclude that copepod secondary production in a summer situation with non-limiting food concentration was best described using a model that solely considers water temperature and copepod body weight.

**KEY WORDS:** Mesozooplankton · Copepod community composition · Density-compensated thermohaline front · Seasonal ice zone · *Calanus* spp. · *Oithona similis* · Copepod growth rate models · Laser optical plankton counter

## 1. INTRODUCTION

Oceanic fronts occur at the boundaries between water masses of different physio-chemical properties such as temperature, salinity, density, nutrients, turbidity and velocity (Bakun 1997). Nutrient-rich water from below the euphotic zone can be resupplied to the surface ocean by upwelling and cross-frontal mixing (Allen et al. 2005). This is the main reason why fronts

often coincide with areas of increased chlorophyll concentration and pelagic primary production (Le Fevre 1987). High numbers of zooplankton and fish larvae have been observed at fronts, due to the accumulation of individuals by convergent flows found in these regions (Franks 1992, Munk et al. 2009). In some cases, reproduction of zooplankton can be favoured, which makes oceanic fronts areas of increased secondary production (Liu et al. 2003, Derisio et al. 2014).

\*Corresponding author: christine.gawinski@uit.no

Depending on the longevity of the front, larger predators are attracted, and energy is effectively channelled through the food web (Acha et al. 2004). Fronts therefore impact trophic transfer efficiency, carbon cycling in the upper layers and export rates to the benthos (Wolanski & Hamner 1988, Hunter & Price 1992, Bakun 1997). They can also act as physical boundaries to the distribution and dispersal of species (Thornhill et al. 2008).

In the Barents Sea, the confluence of warmer, more saline water of Atlantic origin and colder, less saline water of Arctic origin forms the Barents Sea polar front (Sakshaug et al. 2009). The Barents Sea polar front is a density-compensated thermohaline front, meaning that there is no horizontal density gradient that would enhance mixing or upwelling of nutrients (Fer & Drinkwater 2014, Våge et al. 2014). Thus, the front does not lead to increased primary production (Reigstad et al. 2011, Erga et al. 2014) and is therefore a dynamically 'passive' front. However, the Barents Sea polar front is often found coupled with a melt-water front that is the result of sea-ice melt during spring and summer and an important feature promoting primary production. Pelagic blooms in the frontal region occur in 2 phases, one starting near the Barents Sea polar front and progressing northwards, following the retreating ice edge and the resulting stratification (Wassmann et al. 1999). The second phase starts in the southern Barents Sea and moves northwards, resulting in a comparatively slower and less intense bloom which is initiated by stratification caused by near-surface heating from solar radiation (Loeng 1991, Wassmann et al. 1999).

The Barents Sea polar front acts as a habitat boundary for different boreal and arctic species (Hassel 1986, Owrid et al. 2000, Fossheim et al. 2006). One such example is the copepod *Calanus finmarchicus*, a boreal species that is transported into the Barents Sea with the Atlantic current (Hirche & Kosobokova 2007). *C. finmarchicus* has a 1 yr life cycle that is tightly linked to the spring phytoplankton bloom (Conover 1988, Falk-Petersen et al. 2009). Because of the late onset of the phytoplankton bloom in areas north of the polar front and a consequent mismatch with the *C. finmarchicus* reproductive cycle (Tande 1991, Melle & Skjoldal 1998, Aarflot et al. 2018), the polar front acts as a barrier to the successful reproduction of *C. finmarchicus*.

In many historical data sets, an important size fraction (200–800 µm) of the mesozooplankton community, which includes nauplii, copepodites and adults of some smaller species, is significantly underrepresented due to the use of coarse mesh sizes (Gallienne

& Robins 2001). There is growing evidence for the importance of small copepods in Arctic food webs, especially the genus *Oithona*. Newer studies, using appropriate sampling gear, report high abundance, biomass and production at the Barents Sea polar front and in Arctic areas in general (Gallienne & Robins 2001, Turner 2004, Svensen et al. 2011, Zamora-Terol et al. 2013, Basedow et al. 2014, Svensen et al. 2019).

The above-cited studies have increased our knowledge of the distribution of zooplankton at the Barents Sea polar front. Despite the importance of secondary production estimates for evaluating energy transfer in marine food webs, there is still a lack of those estimates across the polar front. To our knowledge, only 2 studies have investigated secondary production across the polar front, one using a laser optical plankton counter (LOPC) in the western Barents Sea (Basedow et al. 2014) and one using a 168 µm meshed Judy net in the eastern Barents Sea (Dvoretsky & Dvoretsky 2024a).

Secondary production is defined as the increase in zooplankton biomass over a period of time and equals the sum of the product of biomass and weight-specific growth rate of each individual stage within the zooplankton population (Runge & Roff 2000). Several methods are used to estimate growth rates, including experimental approaches that determine, for example, the weight-specific egg production rate or measure growth rate directly, as well as field-based cohort-analysis and modelling approaches (Runge & Roff 2000). Technological advances of laser-based instruments to study zooplankton sizes and abundance have led to the possibility of estimating production with a high spatial resolution (Zhou et al. 2010, Basedow et al. 2014). This estimation relies on the so-called biovolume spectrum theory that assumes that biomass or biovolume in marine systems is nearly evenly distributed over logarithmic size classes and that biomass transfer between size classes can be estimated by the slope of the biovolume spectrum (Silvert & Platt 1978, Zhou 2006).

In this study, we investigated mesozooplankton secondary production and community composition with high taxonomic and spatial resolution across the Barents Sea polar front by employing a combination of traditional net sampling using WP-2 nets and GoFlo bottles and optical plankton imaging using the LOPC. To estimate secondary production, we used biomass data from traditional net sampling and optical plankton imaging in combination with empirical growth rate equations from the literature. At present, there is no clear consensus as to the most suitable

growth rate model for application in polar regions, and a careful evaluation of model assumptions and shortcomings is needed before choosing which method to use and interpreting the results. Therefore, our study includes a comprehensive comparison of 4 commonly used growth rate models, namely model A: Hirst & Bunker (2003), model B: Hirst & Lampitt (1998), model C: Huntley & Lopez (1992) and model D: Zhou et al. (2010). We provide a recommendation for the most suitable model to estimate secondary production in high-latitude ecosystems during the summer. Furthermore, we address the following research questions: (1) Is the Barents Sea polar front an area of high secondary production during the summer? (2) Do secondary production and associated mesozooplankton community composition change across the Barents Sea polar front, from warm Atlantic to cold Arctic waters? (3) What are the underlying mechanisms for the observed patterns in secondary production across the front?

## 2. MATERIALS AND METHODS

### 2.1. Study area

Sampling was conducted on board the ice-enforced RV 'Helmer Hanssen' between 22 and 27 June 2011 in the area of Hopen Deep and Great Bank in the Barents Sea (Fig. 1). Station (Stn) M1 (278 m bottom depth) was chosen as a representative location for well-stratified Arctic water masses, Stns M2 (235 m bottom depth) and M3 (282 m bottom depth) were located in the polar front region, and Stn M4 (371 m bottom depth) was located in deep-mixed Atlantic waters.

### 2.2. Environmental data

Hydrography (salinity, temperature and resulting density) profiles were measured at the 4 stations (M1–M4) using a rosette-mounted SBE911plus sys-

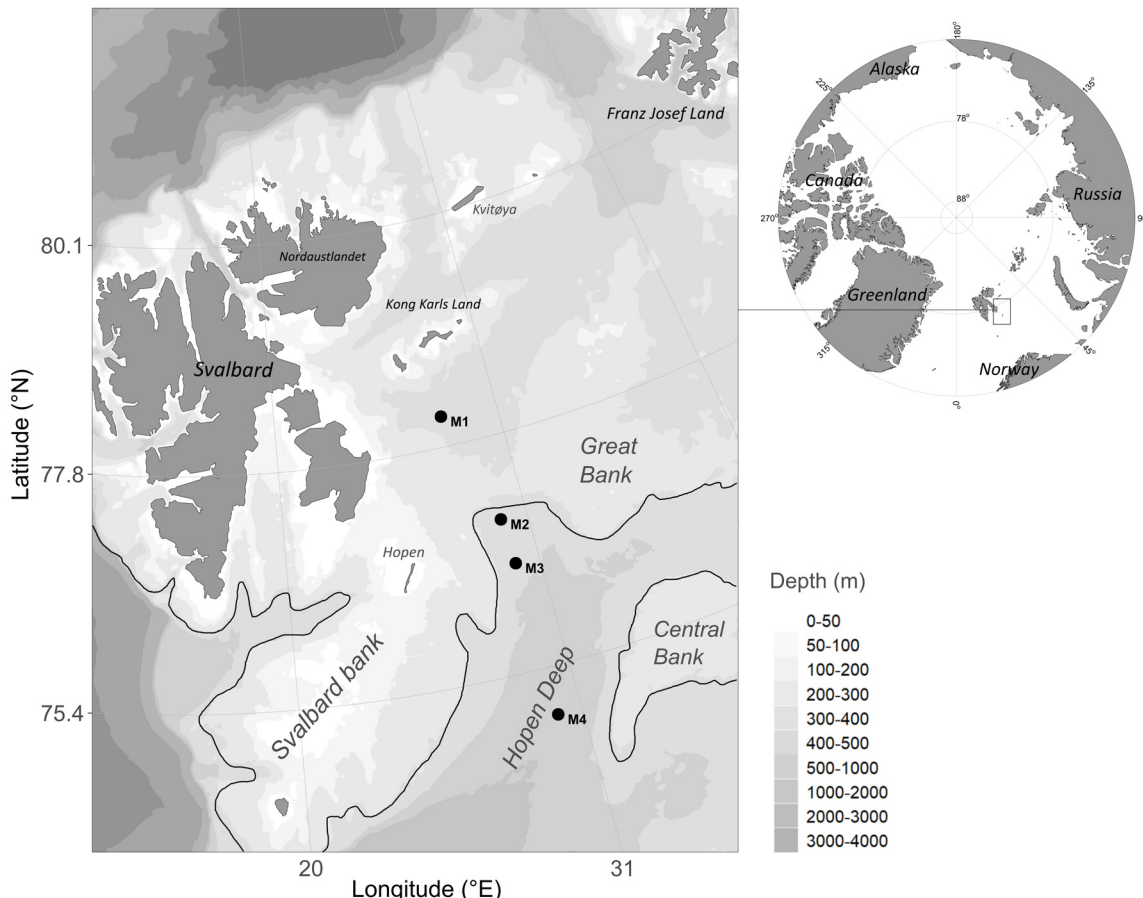


Fig. 1. Study area with the approximate location of the polar front based on the 200 m isobath indicated as a black line. Four stations (M1–M4) were sampled with a WP-2 net and GoFlo bottles, and a transect between these stations was sampled with the laser optical plankton counter (LOPC)

tem (Sea-Bird Electronics). Data were processed following standard procedures as recommended by the manufacturer and averaged to 0.5 m vertical bins before plotting. A moving vessel profiler (MVP; Brooke Ocean Technology), equipped with a CTD (Applied Microsystems Micro CTD), a fluorescence sensor (WET Labs FLRT chl *a* fluorometer) and the LOPC, was used to sample environmental data along the transect. The MVP made close-to-vertical profiles from surface to 10 m above bottom along a transect crossing the polar front. In ice-free waters south of the front, the ship was moving at 6–7 knots, while profiles were taken in MVP 'free-wheel' mode. Farther north, in waters with loose drift ice, the profiles were spaced farther apart and were taken in MVP 'continuous rpm' mode at low vessel speed (1–2 knots). For analyses of salinity, temperature and chlorophyll *a* (chl *a*), data from downward and upward profiles were used. Fluorescence data were converted into chl *a* by scaling the conversion equation supplied by the manufacturer to values obtained from pigment analyses of filtered water samples.

Water for chl *a* determination was collected with Niskin bottles mounted on a rosette at 11 fixed depths: 0, 5, 10, 20, 30, 40, 50, 60, 90, 120 and 200 m. In addition, a 12th depth was sampled at the fluorescence maximum. Triplicate sub-samples of 100–200 ml from each depth were filtered onto Whatman GF/F filters for total chl *a* and 10 µm polycarbonate filters for determination of chl *a* >10 µm. On board the ship, filters were extracted in absolute methanol in darkness for 24 h and then analysed on a Turner Designs 10-AU fluorometer (Holm-Hansen et al. 1965).

### 2.3. Mesozooplankton sampling

#### 2.3.1. WP-2 net and GoFlo bottle sampling

Mesozooplankton were sampled with a WP-2 net (Hydro-Bios) with 180 µm mesh and a net opening with a diameter of 0.57 m and filtering cod-end. Filtration volume was estimated from the opening diameter and the sampling depth. Three vertical net hauls were taken during the day (around noon) and at night (around midnight) at all stations, at fixed depth intervals of 0–50, 50–100 and 100 m to bottom by using a closing mechanism. The content of the cod-end was concentrated over a 90 µm mesh on deck and preserved with buffered formaldehyde at 4% final concentration.

To increase the resolution in the surface and to quantitatively sample the small copepod species and

young developmental stages, one GoFlo profile was sampled in the daytime at each station in the upper 50 m. Samples were taken from 1, 10, 20, 30, 40 and 50 m depth. The content of the water bottle (30 l) from each individual depth was concentrated over a 20 µm mesh and preserved with buffered formaldehyde at 4% final concentration.

Mesozooplankton were counted and determined to species and developmental stage under a Leica dissecting microscope at 40× magnification. *Calanus finmarchicus*, *C. glacialis* and young developmental stages of *C. hyperboreus* were distinguished to species by measuring prosome length of all counted individuals and applying size classes established by Kwasniewski et al. (2003), which are slightly modified in comparison to definitions by Unstad & Tande (1991).

By combining data of zooplankton abundance and taxonomy obtained both with the WP-2 net and the GoFlo bottles, the relative contribution of 'large' and 'small' mesozooplankton can be compared. We followed the definition of Roura et al. (2018), where a total body length of <2 mm defines small copepods. In our data set, 'small copepods' are represented by *Cyclopoida* sp. indet., *Harpacticoida* sp. indet., *Oithona atlantica*, *O. similis*, *Microsetella norvegica*, *Pseudocalanus* spp. and *Triconia borealis*. The group of 'large copepods' is composed of *Calanus finmarchicus*, *C. glacialis*, *C. hyperboreus* and *Metridia longa*. All other and less abundant zooplankton individuals were grouped into 'other zooplankton small' for a size <2 mm and 'other zooplankton large' for a size >2 mm. To get a quantitative representation of both large and small zooplankton across the polar front, data were combined from the WP-2 and GoFlo bottles. 'Other zooplankton small', copepod nauplii, all stages of 'small copepods', as well as all young stages (CI–CIII) of 'large copepods' were obtained from the GoFlo sampling. Data on older stages (CIV–adult) of 'large copepods' and 'other zooplankton large' were obtained from the WP-2 net sampling. To test whether there was a significant difference in copepod community composition between the day- and night-time sampling with the WP-2 net, canonical correspondence analysis was performed on fourth-root transformed abundance data from depth strata 0–50, 50–100 and 100 m to bottom sampled with the WP-2 net during day- or night-time along the transect. The interaction term (station × time of sampling) was included in the model to capture differences in copepod community composition along the transect depending on the time of the day. There was no significant difference between day- and night-time sam-

pling with the WP-2 net (time of sampling:  $p = 0.94$ ; station  $\times$  time of sampling:  $p = 0.983$ ). Therefore, all presented data are based on averaged data from the WP-2 day- and night-time sampling combined with GoFlo bottle sampling. Mesozooplankton abundance was converted into biomass, based on species- and stage-specific carbon weight relationships (Gawinski et al. 2024). The copepod abundance and biomass data are published on GBIF (Gawinski et al. 2023). Mesozooplankton distribution was analysed and visualized using R version 3.6.3.

### 2.3.2. Laser optical plankton counter (LOPC)

The LOPC is designed to count and measure particles in the water column based on laser light that passes a sampling channel and is received on a matrix of photo elements (Herman et al. 2004). The LOPC is currently no longer produced but is still used by research institutes around the world. While the LOPC is being towed through the water, zooplankton and other particles pass through the sampling channel, and their number, size and transparency are recorded. Particles can either occlude 1 or 2 diodes (called single-element particles), or 3 or more diodes (called multi-element particles, MEPs). The size of particles is measured by the peak negative change in voltage detected by each occluded diode and is defined as digital size (DS). The transparency of particles is described by the attenuation index (AI), which is based on the ratio between mean DS of all diodes that are completely occluded by a MEP, and the maximum DS a diode can have. The LOPC provides high-resolution abundance data of mesozooplankton in a size range of 0.25–4 mm. We analysed 3 size groups of particles: small (S, 0.25–0.6 mm equivalent spherical diameter ESD), medium (M, 0.6–1.5 mm ESD) and large (L, 1.5–4 mm ESD). For the medium and large group, we excluded transparent particles ( $AI < 0.4$ ) from our abundance analyses to focus on zooplankton

particles even though we may have missed a fraction of gelatinous plankton that way (Basedow et al. 2014). Mesozooplankton species were separated into the different size classes based on the definitions given by Basedow et al. (2018) (Table 1). LOPC biovolumes were converted into carbon using the regression provided by Forest et al. (2012). Data were collected along the transect and additionally at stations M1–M4, where 4–10 vertical profiles were taken in 'continuous rpm' mode at low vessel speed. The latter data were used to calculate biomass and production estimates of mesozooplankton at the stations. Only data from the downward profiles were used for mesozooplankton analyses.

LOPC particle counts were analysed and quality-controlled as described by Basedow et al. (2014, 2018). The quality of the data was good, with very few (<0.01%) incoherent multi-elements as defined by Schultes & Lopes (2009), meaning the information on the diodes occluded by MEPs was not arranged disorderly. The total number of larger particles was far below  $10^6$ , indicating that the LOPC was not overloaded and counted the correct number of particles (Schultes & Lopes 2009). For particles  $<0.6$ – $0.8$  mm ESD, the LOPC does not allow differentiating zooplankton from other particles, which is possible for larger particles based on their transparency and other features. Therefore, it is often unclear if small particles are zooplankton or detritus (Basedow et al. 2018). Based on a data set from the Mediterranean Sea, Espinasse et al. (2018) developed indicators to designate the contribution of detritus to small particles, by analysing available features of particles in relation to the environment. We used these indicators to determine the contribution of non-zooplankton particles to LOPC counts during our study. For those analyses, all LOPC data, including more transparent particles with an AI  $<0.4$  are necessary and were used. In Atlantic waters south of the polar front, LOPC data were characterized by a low AI of 0.12 and low percentage (<2%) of larger MEPs, which is indicative of

Table 1. Size classification applied to data collected by the laser optical plankton counter (LOPC) at the Barents Sea polar front. Reproductive modes of the different copepod species are indicated as SS for sac spawners and BS for broadcast spawners. ESD: equivalent spherical diameter

Size class	ESD (mm)	Main zooplankton species
Small (S)	0.25–0.6	<i>Oithona</i> spp. (SS), <i>Microsetella norvegica</i> (SS), <i>Triconia</i> spp. (SS), copepod nauplii, Hydrozoa, meroplanktonic larvae, Appendicularia
Medium (M)	0.6–1.5	<i>Pseudocalanus</i> spp. (SS), <i>Calanus</i> spp. CI–CIV (BS), <i>Metridia longa</i> CI–CV (BS), Hydrozoa, Chaetognatha
Large (L)	1.5–4.0	<i>Calanus</i> spp. CV–CVI (BS), <i>Metridia longa</i> CVI (BS), Chaetognatha, juvenile and adult euphausiids

low detritus abundance. North of ca. 76.25° N, across the polar front and in Arctic waters, the data contained a high percentage (>2% or just below) of MEPs and the AI of particles was also low (0.12). In combination with the stratified waters that were observed in this region, this indicates that aggregates contributed to the particles counted by the LOPC in the region north of 76.25° N. As no distinction between particles and zooplankton could be made for size group S in this region, we did not use these data for the calculation of secondary production and excluded this area from our results section.

#### 2.4. Secondary production estimates

Model predictions of copepod secondary production often deviate significantly from direct measurements of copepod growth rates in the field or laboratory (Liu & Hopcroft 2006a,b, Madsen et al. 2008). In addition, different growth rate models provide distinct estimates of secondary production, and each of them has its specific set of assumptions and approximations (Runge & Roff 2000; Table 2). Additionally, a validation of modelled growth rates through field-based growth rate experiments for selected key copepod species at sub-

**Table 2.** Comparison of 3 copepod growth rate models (A–C) and a zooplankton growth rate model (D), including an assessment of the production to biomass (P/B) ratios derived from the different models, with those documented in literature and recommendations for the use of each model. BS: broadcast-spawning; SS: sac-spawning; nd: no data; na: not applicable

	(A) Hirst & Bunker (2003)	(B) Hirst & Lampitt (1998)	Growth rate model	(C) Huntley & Lopez (1992)	(D) Zhou et al. (2010)
Included parameters	Temperature, copepod body weight, chl $\alpha$ concentration	Temperature, copepod body weight	Temperature	Temperature, copepod body weight, chl $\alpha$ concentration	Temperature, copepod body weight, chl $\alpha$ concentration
Copepod groupings	All copepods	All copepods	All copepods	Mesozooplankton	
	Separate equations for SS adults & juveniles, BS adults & juveniles	Separate equations for SS adults & juveniles, BS adults & juveniles			
Data set size	4831 measurements across 88 copepod species within 29 genera	952 measurements across 41 copepod species	181 measurements across 33 species	na <sup>a</sup>	
Percentage of variance explained	35.7% for BS adults; 39% for BS juveniles; 11.3% for SS adults; 28.9% for SS juveniles	43.5% for BS adults, 49.0% for BS juveniles, 31.1% for SS adults, 39.9% for SS juveniles	91%	na <sup>a</sup>	
Applicable temperature range	−2.3 to 30.6°C	−2.3 to 29.0°C	−1.7 to 30.7°C	na <sup>a</sup>	
Applicable copepod body weight	Adults: 0.199–3260 µg C ind. <sup>−1</sup> Juveniles: 0.017–72.1 µg C ind. <sup>−1</sup>	0.075–3620 µg C ind. <sup>−1</sup>	nd	na <sup>a</sup>	
Applicable chl $\alpha$ range	0.016–321.6 mg chl $\alpha$ l <sup>−1</sup>	nd	nd	na <sup>a</sup>	
Estimated P/B ratios	P/B ratio for total copepod community higher than literature values. Best fit for medium and large size classes, overestimation of small size class of mesozooplankton	P/B ratio for total copepod community similar to literature values. Best fit for medium and large size classes, overestimation of small size class of mesozooplankton	P/B ratio for total copepod community similar to literature values. Best fit for medium and large size classes, overestimation of small size class of mesozooplankton	P/B ratio for total copepod community lower than literature values. Best fit for small size class, underestimation of medium and large size class of mesozooplankton	
Recommended use	Estimation of secondary production of large, predominantly herbivorous copepods during food-limiting conditions, e.g. fall and winter	Estimation of secondary production of large, predominantly herbivorous copepods during non-limiting food conditions, e.g. spring and summer. Year-round estimation of secondary production of small, omnivorous copepods	Not recommended in high-latitude ecosystems, due to temperature being the only factor considered and production consequently following temperature trends in the study area	Estimation of mesozooplankton production in combination with biomass data in size bins from optical plankton instruments	

<sup>a</sup>The model of Zhou et al. (2010) originates from the model of Hirst & Bunker (2003) and incorporates the theoretical definition of zooplankton growth by Huntley & Boyd (1984)

zero temperatures is recommended for future studies, and an effort to develop a local growth rate model for high-latitude regions is needed.

Secondary production was estimated for data obtained with the LOPC sampling and with the WP2 net and GoFlo bottle sampling using 2 different methods that cover different parts of the mesozooplankton community. From the WP-2 net and GoFlo bottle sampling, we estimated secondary production for copepods only, as the applied growth rate models are not suitable for zooplankton groups other than copepods (Runge & Roff 2000). We aimed to compare and evaluate existing production models and selected the following models for estimating copepod secondary production in the Barents Sea: model A: Hirst & Bunker (2003), model B: Hirst & Lampitt (1998) and model C: Huntley & Lopez (1992). These are among the most commonly used copepod growth rate models and include important environmental and biological factors, such as temperature, chl  $\alpha$  concentration and copepod body weight, that can be important in governing copepod secondary production (Runge & Roff 2000). Subsequently, we compared the production to biomass (P/B) ratios predicted by the different models to P/B ratios from the literature, to identify the model that proved most suitable for presenting the biological aspects of copepod secondary production across the Barents Sea polar front.

A different approach was applied for data acquired by the LOPC. We estimated mesozooplankton secondary production (including copepods and non-copepod mesozooplankton groups) in different size classes (small, S, 0.25–0.6 mm ESD; medium, M, 0.6–1.5 mm ESD; and large, L, 1.5–4 mm ESD), by applying a zooplankton growth rate model developed for the usage with optical plankton counters (model D: Zhou et al. 2010).

#### 2.4.1. Copepod secondary production based on WP-2 net and GoFlo bottle sampling

Daily copepod secondary production ( $\text{mg C m}^{-3} \text{ d}^{-1}$ ) in the upper 50 m water column was calculated using the following formula (Runge & Roff 2000):

$$p = \sum B_i \times g_i \quad (1)$$

where  $B_i$  is copepod stage-specific biomass for the upper 50 m ( $\text{mg C m}^{-3}$ ), obtained from the WP-2 net and GoFlo bottle sampling, and  $g_i$  is stage-specific growth rate ( $\text{d}^{-1}$ ). We focused on the upper 50 m water column only, as LOPC sampling identified this to be the active mesozooplankton layer.

Ideally, the growth rates of all developmental stages of individual copepod species would be determined experimentally at *in situ* temperatures and food conditions. However, as this would be a tremendous and unrealistically labour-intensive task, different modelling approaches have been developed to estimate growth rates of copepods (Runge & Roff 2000). These models are based on literature reviews of studies that experimentally determine female fecundity and juvenile somatic growth rates of a variety of copepod species. The weight-specific growth is then related to different forcing variables of copepod production, such as temperature, body weight and chl  $\alpha$  concentration. Some of the most widely used examples of growth rate models include:

Model A: Hirst & Bunker (2003), a multiple linear regression growth model that assumes that copepod growth is governed by temperature, copepod body weight and chl  $\alpha$  concentration;

Model B: Hirst & Lampitt (1998), a multiple linear regression model that assumes that copepod growth is dependent on temperature and copepod body weight;

Model C: Huntley & Lopez (1992), a temperature-dependent growth rate model that assumes that copepod growth is solely determined by temperature.

Models A–C (Table S1 in the Supplement at [www.int-res.com/articles/suppl/m735p077\\_supp.pdf](http://www.int-res.com/articles/suppl/m735p077_supp.pdf)) are global copepod growth rate models that can be applied to actively growing copepod populations spanning geographically from polar to tropical regions. The least covered regions in the models are polar offshore areas. Furthermore, most of the models incorporate data from egg production experiments of broadcast-spawning copepods and only include a few *in situ* measurements of juvenile copepod growth rates. Model A is based on the most extensive data set of 4831 weight-specific fecundity and juvenile growth rate measurements, followed by model B with 952 and model C with 181 measurements (Table 2). The temperature range observed during our study was  $-1.4$  to  $4.6^\circ\text{C}$ , the chl  $\alpha$  concentration was  $0.55$ – $1.96 \text{ mg chl } \alpha \text{ m}^{-3}$  (Table S2), and the individual copepod body weight was  $0.06$ – $1317 \mu\text{g C ind.}^{-1}$  (*Oithona* spp. nauplii were the lightest and *Calanus hyperboreus* adult females (AF) the heaviest). Therefore, all variables observed during our study fall well within the application range of the different models (Table 2). To calculate secondary production of broadcast-spawning and sac-spawning copepods, the respective formulas for adult and juvenile copepods of models A and B were used, while model C is applicable to all copepods (Table S1). The copepod sec-

ondary production data are published on GBIF (Gawinski et al. 2023).

#### 2.4.2. Mesozooplankton secondary production based on LOPC data

With the advancement of optical plankton counters, efforts have been made to develop models that can predict growth rates based on biovolume spectrum theory and consider the higher particle abundance observed with optical plankton counters, compared to zooplankton abundance from traditional net sampling. One such example is model D: Zhou et al. (2010), a growth rate model that assumes that growth of zooplankton is governed by temperature, body weight and chl *a* concentration and includes a factor accounting for assimilated food input by zooplankton. This model builds upon the model of Hirst & Bunker (2003) and incorporates the definition of zooplankton growth by Huntley & Boyd (1984), which posits that growth is governed by food concentration, zooplankton assimilation efficiency and clearance rate. By combining the 2 equations and theoretically restructuring the resulting equation, the model is streamlined to require simplified input variables, namely chl *a* concentration, copepod body weight and temperature. By combining these 2 approaches, Zhou et al. (2010) argued that an overestimation of zooplankton growth at high temperatures and food concentrations is avoided. Model D has previously been used to estimate zooplankton secondary production based on the size-bin data from LOPC counts (Basedow et al. 2014). The advantages of estimating secondary production with the LOPC are high spatial resolution and the ability to detect patches of high mesozooplankton secondary production and its extent, depth range and size distribution.

Daily mesozooplankton secondary production ( $\text{mg C m}^{-3} \text{d}^{-1}$ , normalised by size bin) of size classes S, M and L, sampled with the LOPC, was calculated following the method described by Basedow et al. (2014) (their Eqs. 3 & 5). Here, production  $p$  ( $\text{mg C m}^{-3} \text{d}^{-1}$ , normalised by size bin) is given as:

$$p = g \times w \times N \quad (2)$$

where  $g$  is weight-specific growth rate ( $\text{d}^{-1}$ ),  $w$  is mean weight for each size bin ( $\text{mg C ind.}^{-1}$ ), and  $N$  is abundance ( $\text{ind. m}^{-3}$ ). Weight-specific growth  $g$  ( $\text{d}^{-1}$ ) for each size bin was calculated according to Zhou et al. (2010):

$$g(w, T, Chla) = 0.033 \left[ \frac{Chla}{(205 e^{-0.125T})} \right] e^{0.09T} w^{-0.06} \quad (3)$$

where  $w$  is weight for each size bin ( $\text{mg C ind.}^{-1}$ ),  $Chla$  is chl *a* ( $\text{mg C m}^{-3}$ ), and  $T$  is temperature ( $^{\circ}\text{C}$ ). The volume of particles was converted into carbon using a ratio of mg carbon = 0.0475 body volume (Gallienne & Robins 2001), and chl *a* was converted to carbon using a ratio of C:chl *a* = 50 (Basedow et al. 2014).

To compare estimates of copepod secondary production, which are based on biomass obtained from WP-2 net and GoFlo bottle sampling, with mesozooplankton secondary production based on LOPC sampling, we also estimated copepod secondary production using model D. Subsequently, copepod secondary production calculated with models A–D was grouped into 3 size classes ( $S_{\text{net}}$ ,  $M_{\text{net}}$ ,  $L_{\text{net}}$ ), aligning with the size classes used in the LOPC sampling (S, M, L).

#### 2.4.3. Comparison and evaluation of secondary production resulting from different growth rate models

The estimates of copepod secondary production differed considerably when calculated using the 4 selected models (A–D). Overall, model D resulted in the lowest total copepod secondary production values, ranging from 0.11 to 0.27  $\text{mg C m}^{-3} \text{d}^{-1}$  (Stns M2 and M4, respectively, Table 3). The highest total copepod secondary production values were obtained using model A, with 6.48–12.27  $\text{mg C m}^{-3} \text{d}^{-1}$  (Stns M4 and M1, respectively, Table 3), which is 24–84 times higher than using model D (Fig. 2, Table 3). Model B resulted in copepod secondary production values 10–33 times higher, and model C 6–16 times higher values, than model D. Models A and B generally showed the same trend of increasing copepod secondary production from the Atlantic to the Arctic region (models A and B in Fig. 2, Table 3), with highest copepod secondary production observed at the Arctic station (M1) for model A and at the northern station in the polar front (M2) for model B. The opposite trend was observed when using model C, with generally high copepod secondary production in the Atlantic region and in the polar front and lower in the Arctic region (model C in Fig. 2, Table 3). Model D showed highest copepod secondary production in the Atlantic region and lower but comparable copepod production across the polar front and in the Arctic region (model D in Fig. 2, Table 3). For Arctic regions, model A often overestimates the growth rates of juvenile broadcast-spawning copepods by a factor of 3–8 during periods with high chl *a* concentrations (Liu & Hopcroft 2006a,b, Madsen et al. 2008). A large spread of produc-

Table 3. Copepod and mesozooplankton biomass ( $\text{mg C m}^{-3}$ ), estimated copepod and mesozooplankton secondary production ( $\text{mg C m}^{-3} \text{d}^{-1}$ ) averaged for the upper 50 m water column and daily production to biomass (P/B) ratios for copepods and mesozooplankton at 4 stations. Copepod secondary production was estimated according to Hirst & Bunker (2003) (model A), Hirst & Lampitt (1998) (model B), Huntley & Lopez (1992) (model C) and Zhou et al. (2010) (model D) and was based on copepod biomass obtained with WP-2 net and GoFlo bottle sampling. Mesozooplankton secondary production was obtained from laser optical plankton counter (LOPC) counts and the model of Zhou et al. (2010). Copepods and mesozooplankton were divided into size groups (S, small: 0.25–0.6 mm; M, medium: 0.6–1.5 mm; and L, large: 1.5–4 mm) and are depicted as S<sub>net</sub>, M<sub>net</sub>, L<sub>net</sub> for copepods from the WP2-net and GoFlo bottle sampling and S, M, L for mesozooplankton from the LOPC sampling. Production estimates for LOPC size group S at Stns M3, M2 and M1 were excluded due to the contribution of an unknown proportion of non-zooplankton particles

Size class	Station	Region	Biomass		Production				P/B ratio				
			Copepods	Whole meso-zoo-zooplankton community	Copepods		Whole meso-zoo-zooplankton community		Copepods	Whole meso-zoo-zooplankton community			
			Net + GoFlo	LOPC	A	B	C	D	LOPC	A	B	C	D
S <sub>net</sub> / S	M4	Atlantic	4.45	44.31	0.91	0.44	0.34	0.06	0.42	0.20	0.10	0.08	0.01
	M3	Front	6.25	32.33	3.23	1.07	0.31	0.04	No data	0.52	0.17	0.05	0.01
	M2	Front	4.07	30.62	2.10	0.72	0.17	0.01	No data	0.52	0.18	0.04	0.00
	M1	Arctic	12.62	6.73	10.22	2.59	0.49	0.09	No data	0.81	0.21	0.04	0.01
M <sub>net</sub> / M	M4	Atlantic	17.93	24.11	5.52	2.33	1.24	0.21	0.19	0.31	0.13	0.07	0.01
	M3	Front	14.19	16.29	3.89	1.41	0.70	0.09	0.07	0.27	0.10	0.05	0.01
	M2	Front	19.79	14.45	4.94	1.81	0.83	0.06	0.06	0.25	0.09	0.04	0.00
	M1	Arctic	2.27	9.4	0.53	0.16	0.09	0.02	0.01	0.23	0.07	0.04	0.01
L <sub>net</sub> / L	M4	Atlantic	0.42	13.44	0.05	0.03	0.03	0.00	0.08	0.12	0.08	0.08	0.00
	M3	Front	10.41	34.19	1.37	0.66	0.52	0.05	0.13	0.13	0.06	0.05	0.01
	M2	Front	19.25	11.91	2.19	1.12	0.81	0.05	0.04	0.11	0.06	0.04	0.00
	M1	Arctic	14.13	107.01	1.52	0.73	0.54	0.08	0.04	0.11	0.05	0.04	0.01
Total	M4	Atlantic	22.81	81.86	6.48	2.80	1.61	0.27	0.69	0.28	0.12	0.07	0.01
	M3	Front	30.84	82.81	8.49	3.15	1.53	0.18	No data	0.28	0.10	0.05	0.01
	M2	Front	43.10	56.98	9.23	3.65	1.81	0.11	No data	0.21	0.08	0.04	0.00
	M1	Arctic	29.02	123.14	12.27	3.49	1.12	0.19	No data	0.42	0.12	0.04	0.01

tion values for this model can be expected, as it only explains a relatively low percentage of the variance in the data set it is built on (Hirst & Bunker 2003; Table 2). On the other hand, models B and C often seem to underestimate copepod growth rates compared to *in situ* growth rate measurements in Arctic regions (Liu & Hopcroft 2006a,b), although model B explains a higher proportion of the variance in the data set that it is built on (Hirst & Lampitt 1998; Table 2). Model C is probably less suited for Arctic areas, as secondary production by implication follows the pattern of temperature distribution in the study area and does not take copepod stage composition into consideration.

The different size groups (S<sub>net</sub>, 0.25–0.6 mm equivalent spherical diameter [ESD]; M<sub>net</sub>, 0.6–1.5 mm ESD; L<sub>net</sub>, 1.5–4 mm ESD) showed similar trends in relative contribution to total copepod secondary production across models A–C (Fig. 2), but not for model D. Production of size group S<sub>net</sub> was lowest at the Atlantic station (M4) and highest at the Arctic station (M1) for models A–C, while it was the opposite for model D. Size group M<sub>net</sub> showed highest production at Stn M4 and lowest production

at Stn M1 in all models. Size group L<sub>net</sub> had highest production at the northernmost station in the polar front (M2) and lowest production at Stn M4 in models A–C, while for model D, production was equally high at Stns M1 and M4 and lowest at the northernmost station in the polar front (M2) (Fig. 2). The spread in secondary production values across models A–D was largest for the size classes S<sub>net</sub> and M<sub>net</sub> (Fig. 2) and can likely be attributed to the lack of growth rate data of small species and young developmental stages of copepods at high latitudes, and we suggest that this leads to poor predictive power of the models.

To evaluate the performance of the models, we chose to compare daily production to biomass (P/B) ratios of models A–D with P/B ratios from the literature. Alternatively, the predicted growth rates of the individual developmental stages among different copepod species could be compared to experimentally determined growth rate measurements at specific temperatures, as reported in existing literature. However, few studies have conducted these experiments at sub-zero temperatures, limiting the available data for such comparisons. There were clear differences in the daily

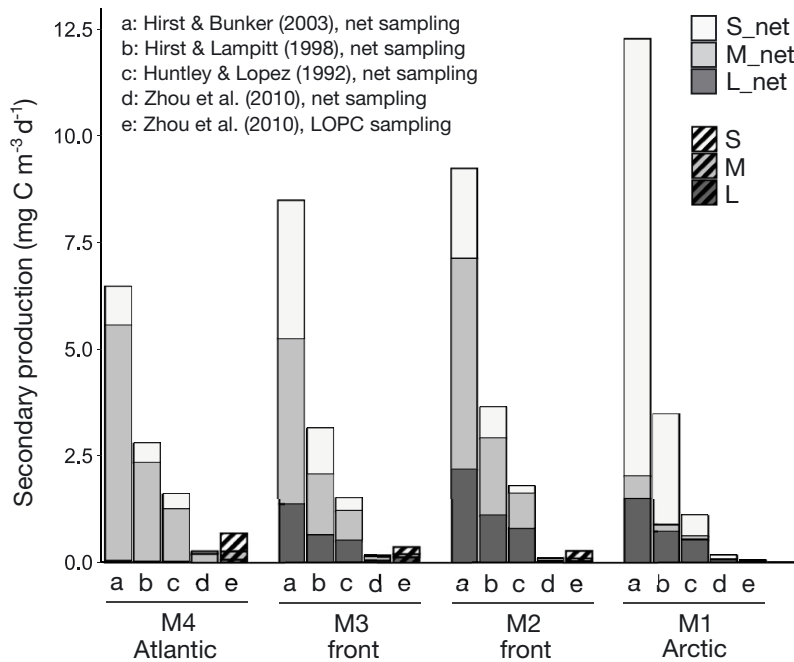


Fig. 2. Copepod (a–d) and mesozooplankton (e) secondary production estimates ( $\text{mg C m}^{-3} \text{ d}^{-1}$ ) averaged over the upper 50 m water column, across the 4 sampling stations (M1–M4) using 5 different methods. a–d are based on copepod biomass estimates from the WP-2 net and GoFlo bottle sampling and the following growth rate models: a: Hirst & Bunker (2003), b: Hirst & Lampitt (1998), c: Huntley & Lopez (1992) and d: Zhou et al. (2010). e is based on laser optical plankton counter (LOPC) mesozooplankton biovolume size spectra and the model of Zhou et al. (2010). Copepods and mesozooplankton were divided into size groups small (S, 0.25–0.6 mm), medium (M, 0.6–1.5 mm) and large (L, 1.5–4 mm) and are depicted as S<sub>net</sub>, M<sub>net</sub>, L<sub>net</sub> for copepods from the WP2-net and GoFlo bottle sampling and S, M, L for mesozooplankton from the LOPC sampling

P/B ratios for the different models (Table 3), with model A showing the highest daily P/B ratios, followed by models B and C, and the lowest daily P/B ratios resulting from model D (Table 3). P/B ratios for specific copepod species in the Arctic are scarce. Daily P/B ratios of the large copepod *C. glacialis* (size group L) ranged between 0.03 and 0.05 d<sup>-1</sup> in the Arctic (Slagstad & Tande 2007). Yearly P/B ratios of 6.5 yr<sup>-1</sup> for *C. finmarchicus* and 3.25 yr<sup>-1</sup> for *C. glacialis* and *C. hyperboreus* have been reported for the Barents Sea (Pedersen et al. 2021). When assuming a growth period of 150 d (June to August, as used for the annual biomass calculations in Pedersen et al. 2021), this results in daily P/B ratios of 0.04 for *C. finmarchicus* and 0.02 for *C. glacialis* and *C. hyperboreus*. Daily P/B ratios for the small copepod *Pseudocalanus* sp. (size group S) range between 0.007 and 0.043 d<sup>-1</sup> (Sakshaug et al. 2009). Yearly P/B ratios of 6.5 yr<sup>-1</sup> for small copepods (Pedersen et al. 2021) and 2.7 yr<sup>-1</sup> for *Pseudocalanus* sp. (Sakshaug et al. 2009) have been reported. These yearly ratios result in daily P/B ratios of 0.01–0.02 (assuming a 365 d growth period). Daily P/B ratios for

the total mesozooplankton community in the Barents Sea varied between 0.02 and 0.10 (Dvoretsky & Dvoretsky 2009, 2024a,b). The P/B ratios of the total copepod community and size group L<sub>net</sub> based on models B and C in this study match the literature values, while the P/B ratios of model A were higher and those of model D were lower (Table 2). For size group S<sub>net</sub>, models A–C gave higher P/B ratios than the ones reported in the literature, while model D gave similar results (Table 2).

Based on the observations outlined above, we suggest that the 2 temperature-dependent models, B and C, describe copepod secondary production most realistically in summer. By including a body weight factor, model B takes copepod stage composition into consideration and is therefore a better representation of copepod secondary production than model C. Early life stages of copepods grow faster than adults (Hirst & Lampitt 1998), which is not taken into consideration in the latter model. Model B approximates the maximum possible copepod growth at certain temperatures under food saturation, and we suggest it

should be used to estimate copepod secondary production in Arctic regions during spring and summer months. During periods with low ch<sub>a</sub> concentrations, model A might be a better approximation of the growth of predominantly herbivorous copepods, e.g. *Calanus* spp., as they would likely be food limited. For small, omnivorous copepods, model B is a good approximation of growth throughout the year, as the growth of these copepods is generally more temperature limited than food limited. Based on the argumentation outlined above, the main results of copepod secondary production across the polar front are based on WP-2 net and GoFlo bottle sampling combined with model B (Table 2).

The average LOPC-derived mesozooplankton secondary production for the upper 50 m (based on LOPC counts and model D) was lower than the copepod secondary production (based on WP-2 net and GoFlo bottle sampling) estimated with models A–C, but was higher than the copepod secondary production when estimated with model D. This means that the traditional copepod growth rate models (A–C)

result in higher growth rates compared to the optical plankton counter growth rate model (D). However, the LOPC showed concentrated patches of extremely high mesozooplankton secondary production along the transect, where the magnitude was comparable to the average copepod secondary production obtained with traditional net sampling and model B (see Figs. 5 & 7). If mesozooplankton secondary production in these patches were calculated with model B, these values would have been several orders of magnitude higher than copepod secondary production obtained from traditional net sampling. To evaluate the spatial distribution, depth range and patchiness of mesozooplankton secondary production across the Barents Sea polar front, we present results based on LOPC sampling combined with model D.

### 3. RESULTS

#### 3.1. Hydrography and chl $\alpha$

A thorough description of hydrography, small-scale current shear, diffusivity, suspended chl  $\alpha$  biomass and dominant phytoplankton taxa at the polar front in June 2011 is provided by Wiedmann et al. (2014). Here we present a short summary of results relevant to this study.

The polar front was identified between approximately 76.3° and 77.5° N and was characterized by the confluence of Arctic water (ArW, temperature [T] < 0°C, 34.3 < salinity [S] < 34.8, Loeng 1991) and Atlantic water (AW, T > 3°C, S > 35.0, Loeng 1991). Very open drift ice with a coverage of around 30% was only observed at Stn M1 during the sampling period, while Stns M2–M4 were ice-free. The water column at M1 was characterized by a shallow, cold, low-salinity surface mixed layer, about 7 m thick. Temperatures were low throughout the water column, exceeding zero only at depths greater than 200 m (Fig. 3A). At Stn M2, a 15 m thick surface mixed layer with even lower salinity was observed, likely reflecting larger total meltwater input. Modified AW was found below 85 m. At Stn M3, an 18 m thick surface mixed layer was followed by a sharp increase in salinity and decrease in temperature, down to a thin layer with remnants of ArW (around 20–40 m depth). There was a rapid transition to AW at a depth of 50 m, with temperature peaking at 3°C at 75 m depth. Stn M4 was situated inside the AW domain, where a deep (~30 m) surface mixed layer with T > 5°C was observed.

The concentration of chl  $\alpha$  across the polar front was patchy (Fig. 3C). Subsurface chl  $\alpha$  maximum concen-

trations were found at all stations well below the mixed layer depth. The highest concentration of extracted chl  $\alpha$ , 4.4 mg m<sup>-3</sup>, was found in the Arctic region (Stn M1, 40 m depth), while the maximum across the front and in the Atlantic region ranged from 1.4 to 2 mg chl  $\alpha$  m<sup>-3</sup> (between 30 and 40 m depth). The Arctic region (Stn M1) was different from the other areas by having a bloom of larger cells >10 µm, while cells <10 µm prevailed in the rest of the study area (Table S2). Integrated mean chl  $\alpha$  concentrations for the upper 50 m water column ranged from 1.96 mg chl  $\alpha$  m<sup>-3</sup> in the Arctic region (Stn M1) to 0.55–0.90 mg chl  $\alpha$  m<sup>-3</sup> across the front (Stns M2 and M3, respectively) and 0.82 mg chl  $\alpha$  m<sup>-3</sup> in the Atlantic region (Stn M4) (Table S2).

#### 3.2. Mesozooplankton community composition and secondary production across the Barents Sea polar front

##### 3.2.1. Spatial resolution of mesozooplankton distribution using LOPC sampling

High-resolution sampling with the LOPC revealed a patchy distribution of mesozooplankton across the polar front. Overall, mesozooplankton abundance was highest in the Atlantic region (Stn M4) and decreased across the polar front (Stns M3, M2), with lowest numbers observed in the Arctic region (Stn M1) (Fig. 4). Small-sized particles (zooplankton) of 0.25–0.6 mm ESD (size group S) were most abundant in the Atlantic region, where they reached maximum numbers of 560 000 ind. m<sup>-3</sup> and were distributed throughout the whole water column. High numbers of small-sized particles (zooplankton and aggregates) were also observed in the northern parts of the polar front, from approximately 76.7° to 77.5° N, where they were located in the surface layers to a depth of about 100 m (Fig. 4). Medium-sized zooplankton particles of 0.6–1.5 mm ESD (size group M, Fig. 4) and large-sized zooplankton particles of 1.5–4 mm ESD (size group L, Fig. 4) were distributed more patchily and reached maximum numbers of 105 000 and 4800 ind. m<sup>-3</sup>, respectively. A patch of medium-sized zooplankton with high abundance was found associated with the sub-surface chl  $\alpha$  maximum in the Atlantic region. A patch of large-sized zooplankton was observed associated with an area of warmer water, located below the tongue of the polar front south of Stn M3 (Fig. 4). Along the rest of the transect, medium- and large-sized zooplankton were less abundant.

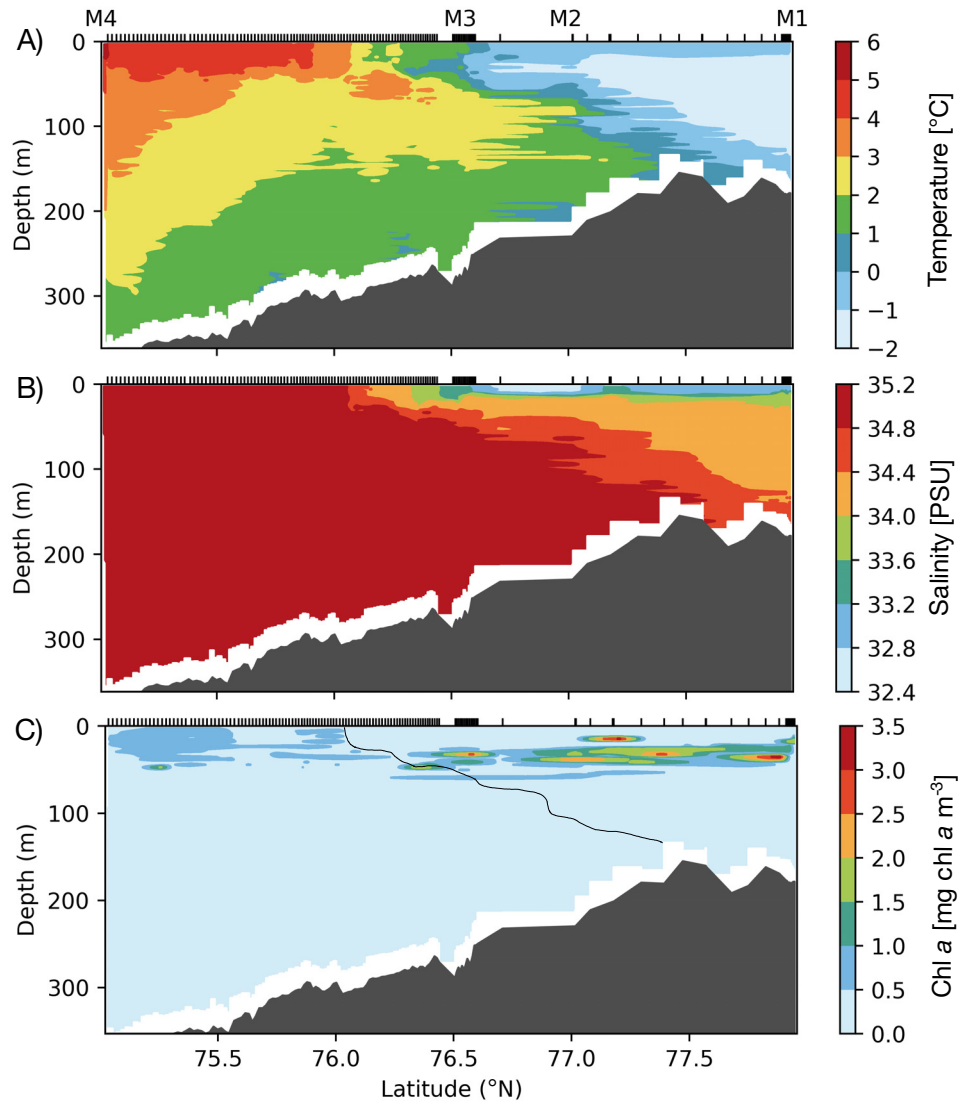


Fig. 3. Transect of (A) temperature ( $^{\circ}\text{C}$ ), (B) salinity (PSU) and (C) chlorophyll *a* concentration ( $\text{mg chl } \text{a } \text{m}^{-3}$ ) across the polar front from Hopen Deep (left) to Great Bank, Barents Sea (right), in June 2011. The approximate location of the polar front based on the 34.8 isohaline is indicated with a black line. The locations of the different profiles are indicated with black dashes

### 3.2.2. Spatial resolution of mesozooplankton secondary production

Mesozooplankton secondary production (based on LOPC sampling combined with growth rate model D, Zhou et al. 2010) was mainly concentrated in the upper 50 m water column. Total mesozooplankton secondary production was highest in the Atlantic region and lower across the polar front and in the Arctic region (Fig. 5, mesozooplankton production values from panels A–C combined). In the Atlantic region, mesozooplankton secondary production of size group S reached a maximum of  $1.2 \text{ mg C m}^{-3} \text{ d}^{-1}$  in localized patches and averaged  $0.42 \text{ mg C m}^{-3} \text{ d}^{-1}$  for the upper 50 m (Stn M4, Table 3), which constituted a large proportion of the total mesozooplankton secondary pro-

duction in this area (Fig. 5). For the region north of  $76.35^{\circ}\text{N}$ , we cannot report accurate mesozooplankton production values for size group S, due to an unknown contribution of non-zooplankton particles. The estimates of size group S in this area approximate the maximum possible mesozooplankton secondary production, including the unknown contribution of detritus. These values are lower than the values observed in the Atlantic region, meaning that the Atlantic region was the most productive area during our study. Mesozooplankton secondary production of size groups M and L was patchily distributed across the transect and associated with areas of high chl *a* concentrations (Fig. 5). The average mesozooplankton secondary production in the upper 50 m of size groups M and L was highest in the Atlantic region and the southern part of the polar

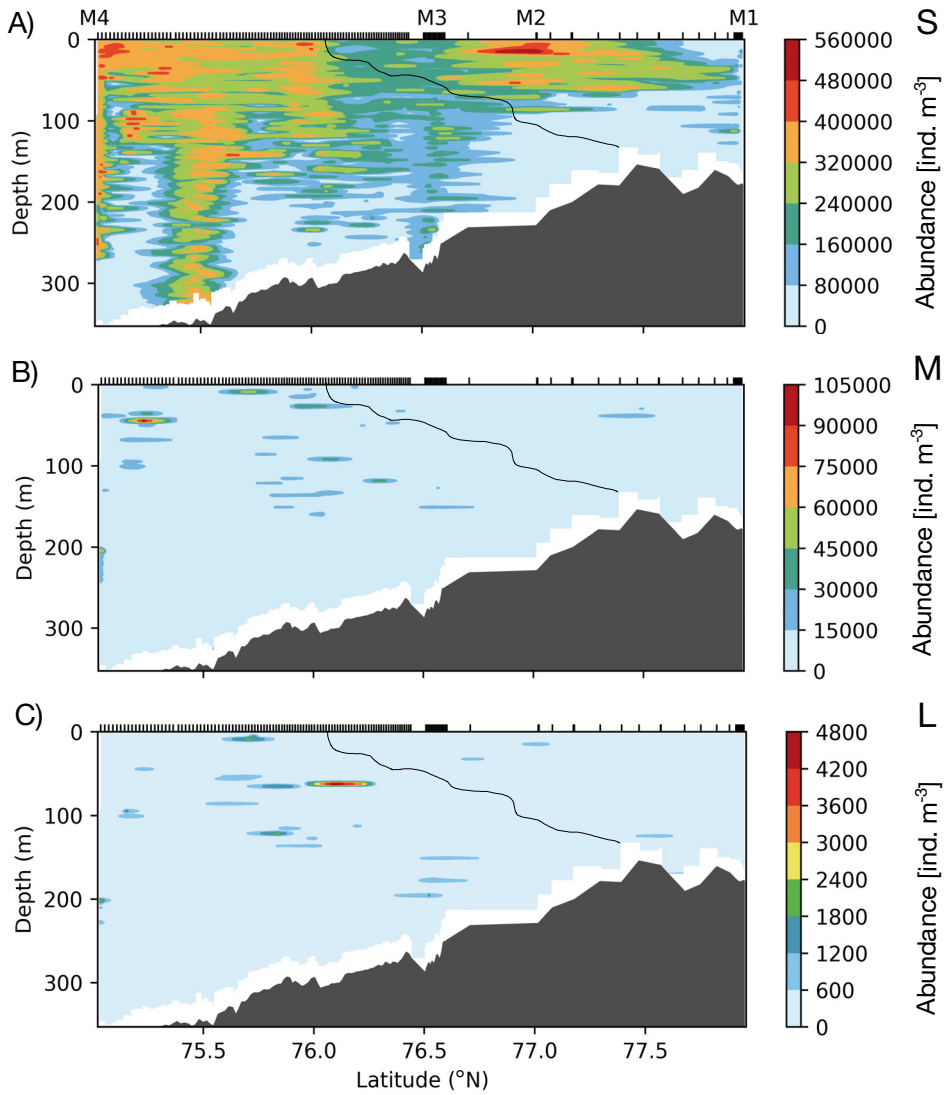


Fig. 4. Transect of mesozooplankton abundance ( $\text{ind. m}^{-3}$ ) obtained with the laser optical plankton counter (LOPC) across the polar front from Hopen Deep (left) to Great Bank, Barents Sea (right). (A) Small-sized particles (S, 0.25–0.6 mm equivalent spherical diameter, ESD), (B) medium-sized particles (M, 0.6–1.5 mm ESD), (C) large-sized particles (L, 1.5–4.0 mm ESD). The approximate location of the polar front based on the 34.8 isohaline is indicated with a black line. The locations of the different LOPC profiles are marked with black dashes, and M1–M4 mark the locations where WP-2 net and GoFlo samples were taken

front, with  $0.19 \text{ mg C m}^{-3} \text{ d}^{-1}$  (Stn M4, Table 3) and  $0.13 \text{ mg C m}^{-3} \text{ d}^{-1}$  (Stn M3, Table 3), respectively. Some small patches of size groups M and L reached maximum values of  $1.75$  and  $3.5 \text{ mg C m}^{-3} \text{ d}^{-1}$ , respectively.

### 3.2.3. Taxonomic resolution of mesozooplankton distribution using WP-2 net and GoFlo bottle sampling

Total mesozooplankton abundance from the WP-2 net and GoFlo sampling was highest in the Atlantic region (Stn M4) and decreased across the polar front towards the Arctic region (Stn M1) (Fig. 6A). The

lowest mesozooplankton abundance was observed in the northern part of the polar front (Stn M2). Between 95 and 98% of all mesozooplankton individuals were found in the surface layer from 0 to 50 m depth (Fig. 6A). Total mesozooplankton biomass in the upper 50 m ranged from  $22.81 \text{ mC m}^{-3}$  in the Atlantic region (Stn M4) to  $43.10 \text{ mg C m}^{-3}$  in frontal waters (Stn M2, Table 2) and was dominated by large copepods of the genus *Calanus* (Fig. 6D). Calanoid copepod nauplii contributed considerably to total mesozooplankton biomass in the Arctic region, while young developmental stages (CI–CIV) and small-sized copepods contributed most to total mesozooplankton biomass in the Atlantic region (Fig. 6E).

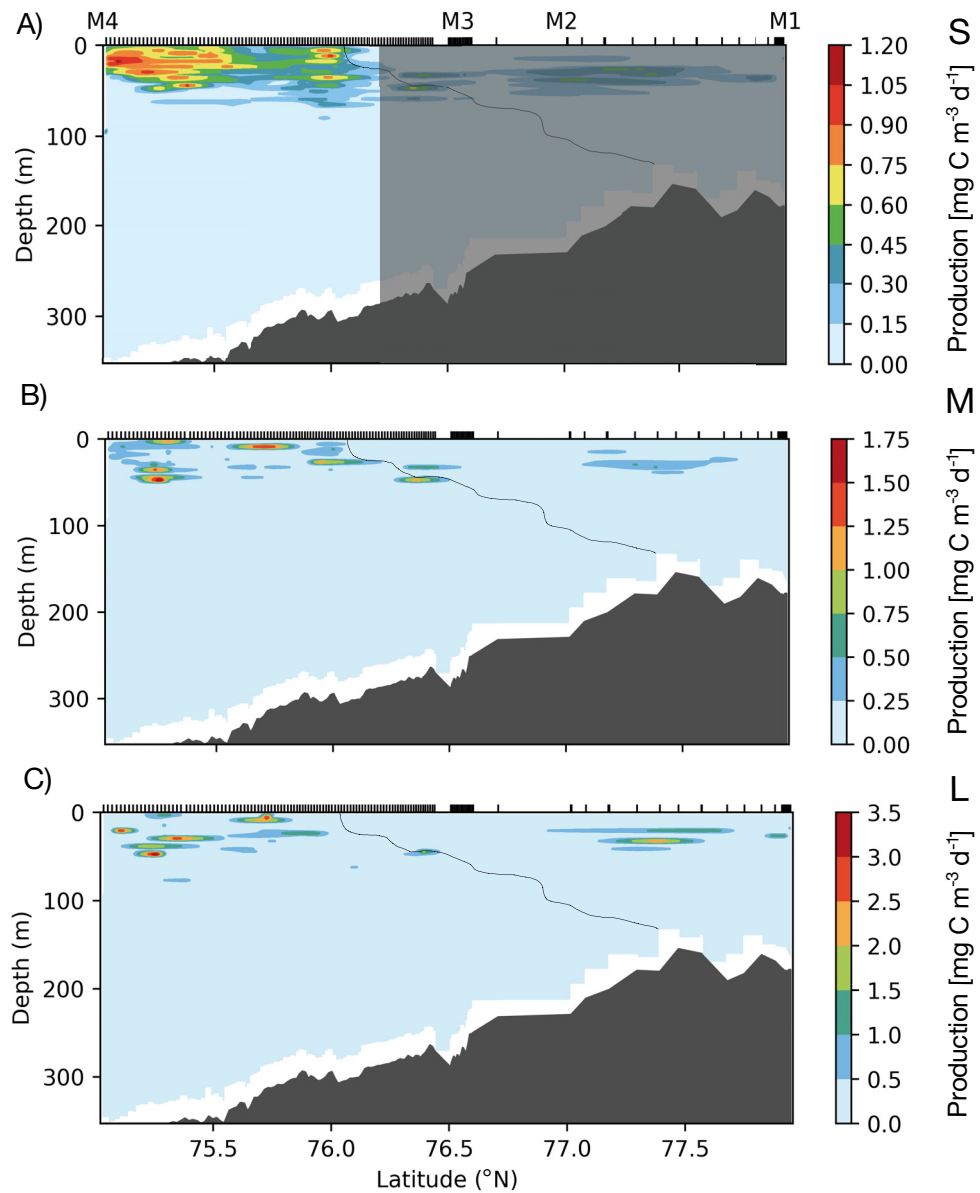


Fig. 5. Transect of mesozooplankton secondary production ( $\text{mg C m}^{-3} \text{d}^{-1}$ ) across the Barents Sea polar front based on the laser optical plankton counter (LOPC) data. (A) Small-sized particles (S, 0.25–0.6 mm equivalent spherical diameter, ESD). Estimations north of  $76.25^\circ \text{N}$  are excluded from the results, as a possible overestimation of production, due to an unknown fraction of aggregates contributing to the LOPC counts in this region, cannot be ruled out (grey shaded area). (B) Medium-sized particles (M, 0.6–1.5 mm ESD). (C) Large-sized particles (L, 1.5–4.0 mm ESD). The approximate location of the polar front based on the 34.8 isohaline is indicated with a black line. The locations of the different LOPC profiles are marked with black dashes, and M1–M4 mark the locations where WP-2 net and GoFlo samples were taken

When considering the combined abundance of copepod and non-copepod mesozooplankton in the Atlantic region (Stn M4), Rotifera and copepod nauplii accounted for 49 and 39% of the total abundance, respectively (Fig. 6A–C). Across the polar front and in the Arctic region, copepod nauplii were the dominant mesozooplankton group, accounting for 68–71% of total abundance. Small cyclopoid and harpacticoid copepods and their nauplii were more abundant in the south, with abundance of *Oithona similis* decreasing

from  $3.4 \times 10^3 \text{ ind. m}^{-3}$  in the Atlantic region (Stn M4) to  $0.6 \times 10^3 \text{ ind. m}^{-3}$  in the Arctic region (Stn M1). Large copepods were numerically dominated by *C. finmarchicus* in the south (99%) and *C. glacialis* in the north (95%, data not shown). Across the polar front, a mix of both *Calanus* species was observed (between 79 and 87% *C. finmarchicus*). *C. hyperboreus* was absent in the Atlantic region (Stn M4) and only found in very low abundance across the polar front (0.1–0.2%), while it contributed 5% to total *Calanus* spp. abun-

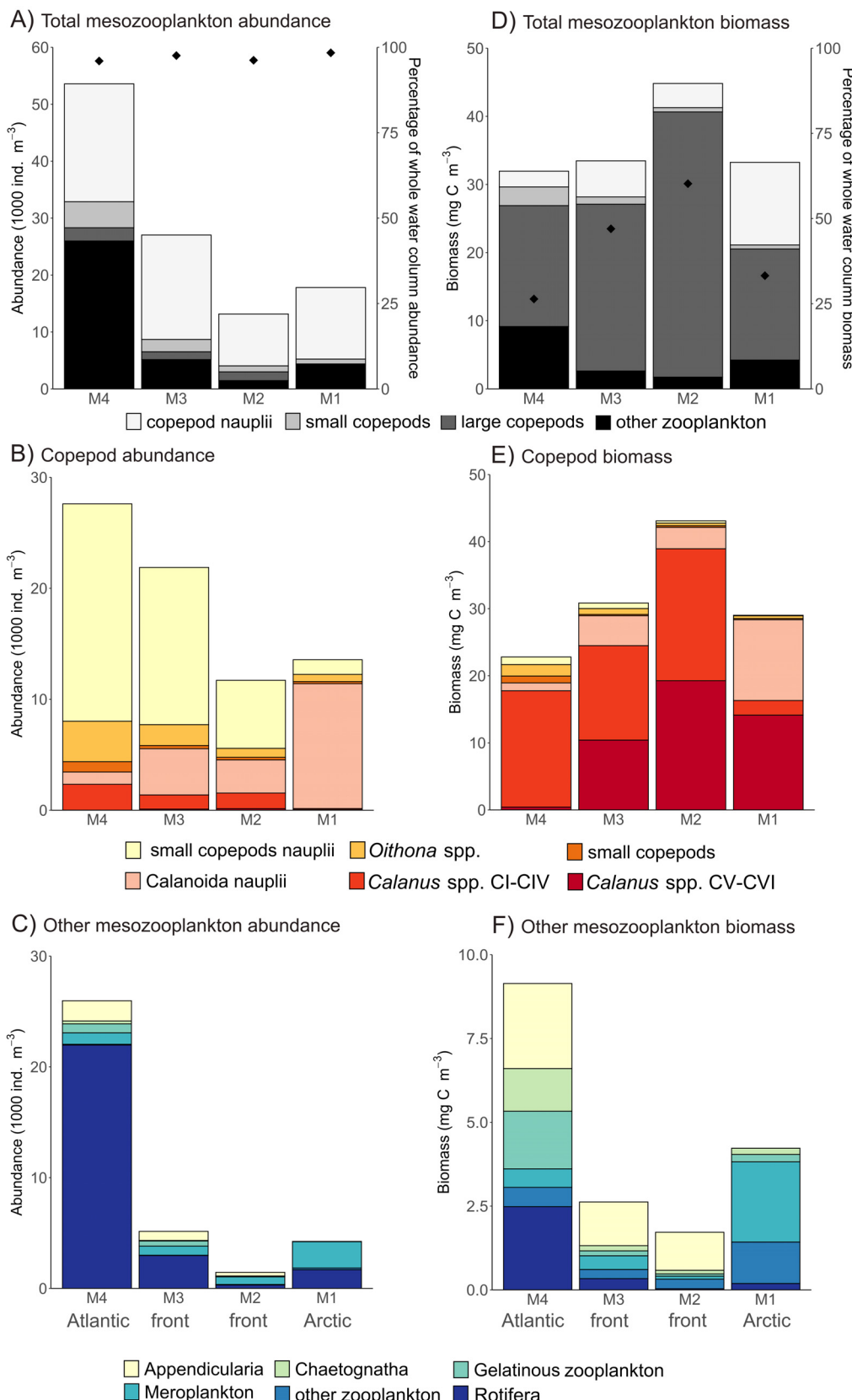


Fig. 6. Abundance (upper 50 m, 1000 ind. m<sup>-3</sup>) of (A) total mesozooplankton, (B) copepods and (C) mesozooplankton other than copepods, and biomass (upper 50 m, mg C m<sup>-3</sup>) of (D) total mesozooplankton, (E) copepods and (F) mesozooplankton other than copepods collected with the WP-2 net and GoFlo bottles at the sampling stations (M1–M4) across the polar front. The right axes in panels A and D indicate the percentage of the whole water column abundance and biomass that is found in the upper 50 m at each station, respectively (indicated by diamonds). Note the different scales on the y-axes

dance in the Arctic region (Stn M1). The *Calanus* community was in an early developmental state in the Arctic region, where active reproduction was observed, and the community was dominated by adults and CV copepodites (1 and 32%, respectively, Fig. 6E). Crossing the polar front into the Atlantic region, the *Calanus* community gradually showed a more advanced developmental state, and the contribution of young stage CI–CIV copepodites increased from 67 to 100 % (Stns M1 to M4). Zooplankton other than copepods contributed a high proportion to total mesozooplankton abundance in the upper 50 m. Here, Rotifera, with *Synchaeta* spp. as the main representative, and Appendicularia, with *Fritillaria borealis* as the main representative, were most abundant, with  $22 \times 10^3$  and  $1.8 \times 10^3$  ind.  $m^{-3}$  in the Atlantic region (Stn M4), respectively (Fig. 6C,F). Appendicularia, Chaetognatha and gelatinous zooplankton were abundant in the Atlantic region but were almost completely absent in the Arctic region. High numbers of larval stages of Polychaeta, Echinodermata and Bivalvia were observed at the Arctic region (Stn M1) and in the northern parts of the polar front (Stn M2) (Fig. 6).

### 3.2.4. Taxonomic resolution of copepod secondary production

Estimates of the total copepod secondary production (based on WP-2 and GoFlo sampling and model B, Hirst & Lampitt 1998) ranged from  $2.80 \text{ mg C m}^{-3} \text{ d}^{-1}$

in the Atlantic region (Stn M4) to  $3.65 \text{ mg C m}^{-3} \text{ d}^{-1}$  in the northern sector of the polar front (Stn M2) and  $3.49 \text{ mg C m}^{-3} \text{ d}^{-1}$  in the Arctic region (Stn M1) (Table 4, Fig. 7).

Of the total copepod production, the small copepods and nauplii (size group S<sub>net</sub>) contributed the least at Stn M4, with  $0.45 \text{ mg C m}^{-3} \text{ d}^{-1}$ , but their production increased northwards, reaching a maximum of  $2.59 \text{ mg C m}^{-3} \text{ d}^{-1}$  in the Arctic region (Stn M1) (Fig. 7, Table 4). In the Atlantic region, the small copepods *Oithona similis*, *Microsetella norvegica* and *Triconia borealis* and their nauplii together contributed 33.3% to copepod secondary production of size group S<sub>net</sub>. In the rest of the transect, copepod secondary production of size group S<sub>net</sub> was completely dominated by calanoid nauplii (96–99%). Copepod secondary production of size group M<sub>net</sub> was highest in the Atlantic region (Stn M4) with  $2.32 \text{ mg C m}^{-3} \text{ d}^{-1}$  and decreased across the polar front to a minimum of  $0.16 \text{ mg C m}^{-3} \text{ d}^{-1}$  in the Arctic region (Stn M1) (Fig. 7, Table 4). Reflecting the *Calanus* spp. community composition, copepod secondary production of size group M<sub>net</sub> was mainly comprised of *C. finmarchicus* CI–CIV copepodites in the south (Stn M4), while *C. glacialis* CI–CIV copepodites gained in importance crossing the front and were the main contributors in the Arctic region (Stn M1). Copepod secondary production of size group L<sub>net</sub> was lowest in the Atlantic region (Stn M4) with  $0.03 \text{ mg C m}^{-3} \text{ d}^{-1}$  and reached  $0.74 \text{ mg C m}^{-3} \text{ d}^{-1}$  in the Arctic region (Stn M1) (Fig. 7, Table 4). The *Calanus* spp.

**Table 4.** Copepod secondary production estimates (prod.) in  $\text{mg C m}^{-3} \text{ d}^{-1}$  for the upper 50 m water column, based on the growth rate model of Hirst & Lampitt (1998), and percentage of total copepod secondary production (% prod.) for different categories of copepods at the Atlantic station (M4), the frontal stations (M3 and M2) and the Arctic station (M1). Depicted are total copepod secondary production (all stages CI–CVI + nauplii), secondary production of copepod nauplii (Calanoida and Cyclopoida & Harpacticoida nauplii) and secondary production of copepod stages CI–CVI (small copepods CI–VI, large copepods CI–IV, large copepods CV–CVI). Size classification of the different copepod categories is depicted as S<sub>net</sub>, M<sub>net</sub> and L<sub>net</sub>

	— Atlantic — (Stn M4)		Front		— Arctic — (Stn M1)	
	Prod.	% prod.	Prod.	% prod.	Prod.	% prod.
Copepod nauplii + CI–CVI	2.80	100	3.15	100	3.65	100
Copepod nauplii	0.36	12.8	1.04	33.0	0.71	19.5
Calanoida nauplii (S <sub>net</sub> )	0.30	10.7	1.01	32.0	0.70	19.2
Cyclopoida, Harpacticoida nauplii (S <sub>net</sub> )	0.06	2.1	0.03	1.0	0.01	0.3
Copepods CI–CVI	2.44	87.2	2.11	67.0	2.94	80.5
Small copepods	CI–VI (S <sub>net</sub> )	0.09	3.2	0.04	1.3	0.01
Large copepods	CV–VI (L <sub>net</sub> )	0.03	1.1	0.66	20.9	30.6
	CI–IV (M <sub>net</sub> )	2.32	82.9	1.41	44.8	1.81
					49.6	0.16
						4.6

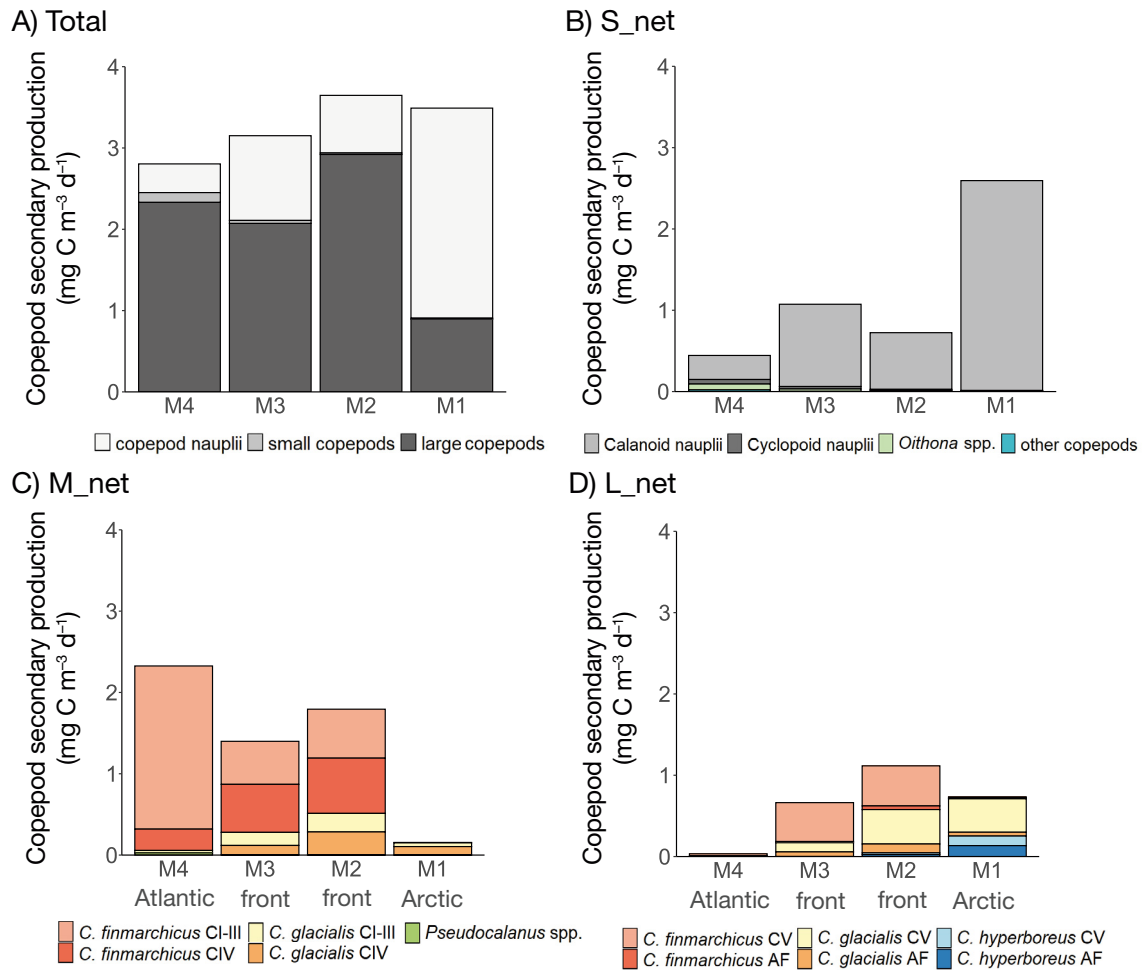


Fig. 7. Copepod secondary production estimates (averaged for the upper 50 m,  $\text{mg C m}^{-3} \text{d}^{-1}$ ) based on WP-2 net and GoFlo sampling for the different size classes of copepods according to the model of Hirst & Lampitt (1998). (A) Total copepod secondary production, (B) small size class ( $S_{\text{net}}$ ), (C) medium size class ( $M_{\text{net}}$ ), (D) large size class ( $L_{\text{net}}$ ). AF: adult females

community composition was reflected in the copepod secondary production of size group  $L_{\text{net}}$ , with *C. finmarchicus* CV and AF contributing most to copepod secondary production in the southern parts of the transect (Stns M4 and M3), while *C. glacialis* and *C. hyperboreus* CV and AF contributed most in the northern parts (Stns M2 and M1).

#### 4. DISCUSSION

While the Barents Sea is often considered to be a highly productive area, few studies have addressed the quantity and pattern of mesozooplankton secondary production in this area, despite the undeniable importance of mesozooplankton for the energy transfer in marine food webs. In this study, we investigated mesozooplankton and specifically copepod secondary production with high taxonomic and spatial res-

olution across the Barents Sea polar front in summer, by utilizing a combination of traditional net sampling and optical plankton imaging techniques. The LOPC was a useful tool for detecting patches of high mesozooplankton secondary production and provided valuable information about the extent, depth range and size distribution of the productive mesozooplankton layer. We found a distinct pattern of secondary production across the front, where total mesozooplankton secondary production (including copepod and non-copepod groups) was mainly concentrated in the upper 50 m water column and was highest in the Atlantic region south of the polar front. Copepods and their nauplii were the main component of the mesozooplankton community across the whole study region. In the Atlantic region, however, high abundance and biomass of other mesozooplankton groups, such as Rotifera, Chaetognatha, and Appendicularia, were observed. Copepod secondary production was

lowest in the Atlantic region and increased towards the Arctic region. Different copepod species and life stages played an important role for copepod secondary production in distinct regions of the polar front and were influenced by varying environmental and biological factors across the study area. For our copepod secondary production estimates, we decided to use the model of Hirst & Lampitt (1998) (considering temperature and copepod body weight), because we believe that it best approximates the growth of copepods under food saturation and low temperatures found in the study area.

#### 4.1. Is the Barents Sea polar front an area of increased secondary production?

The Barents Sea is an Arctic shelf sea known for its high productivity and contrasting production regimes in its northern parts, influenced by cold, Arctic water and its southern parts, influenced by warm, Atlantic water (Sakshaug et al. 2009). Secondary production in the study region is influenced by the advection of zooplankton biomass with the Norwegian Atlantic Current (Wassmann et al. 2006), by the interplay of sea-ice retreat, the meltwater front and the phytoplankton bloom status (Wassmann et al. 1999), and by predation pressure (Langbehn et al. 2023). Total mesozooplankton secondary production at the end of June was highest in the Atlantic region south of the Barents Sea polar front (Fig. 5), which is in accordance with results from a previous study conducted with the LOPC in the same area in summer (Basedow et al. 2014). The secondary production values of the mesozooplankton community reported by Basedow et al. (2014) for the Atlantic region in August were substantially higher than the ones reported in the present study for the end of June. During the study of Basedow et al. (2014), a late summer bloom was occurring in the Atlantic region, indicated by a maximum surface chl *a* concentration of  $2.8 \text{ mg m}^{-3}$ , which might have promoted increased levels of secondary production in the region.

Copepod secondary production during our study, on the other hand, was lowest in the Atlantic region and increased towards the north, reaching a maximum in the northern part of the polar front (Stn M2, Fig. 7). In the eastern Barents Sea, highest copepod secondary production was also recorded in the Barents Sea polar front in summer (Dvoretsky & Dvoretsky 2024a). In the present study, total copepod secondary production was  $2.8 \text{ mg C m}^{-3} \text{ d}^{-1}$  in the Atlantic region,  $3.15\text{--}3.65 \text{ mg C m}^{-3} \text{ d}^{-1}$  across the polar

front and  $3.49 \text{ mg C m}^{-3} \text{ d}^{-1}$  in the Arctic region (upper 50 m, growth rate model of Hirst & Lampitt 1998), and higher than previously reported for the Barents Sea (Dvoretsky & Dvoretsky 2009, 2012, 2024a,b; Table 5). Copepod secondary production reported in the present study was also higher than production in other Arctic regions in summer months, such as in Disko Bay, western Greenland (Madsen et al. 2001, 2008; Table 5), the Bering Sea (Kimmel et al. 2018; Table 5) and the Gulf of Alaska (Coyle & Pinchuk 2003; Table 5). Secondary production reported for the White Sea (Primakov & Berger 2007; Table 5) and Chukchi Sea (Sastri et al. 2012; Table 5) was higher, but here different methodology was used, namely the physiological method and the chitobiase essay, respectively, and the production values are therefore not directly comparable. We conclude that the north-western Barents Sea is generally a very productive region in summer, but the polar front itself is not an area with increased total mesozooplankton secondary production, but rather increased copepod secondary production.

There are at least 2 possible reasons for the high total mesozooplankton production combined with low copepod production in the Atlantic region, namely advection of zooplankton biomass, resulting in high predation risk for large copepods, and differences in food availability across the polar front. Firstly, zooplankton abundance and biomass in the Atlantic part of the Barents Sea are highest in summer and strongly influenced by the advection of organisms from the Norwegian Sea into the Barents Sea (Wold et al. 2023). During this period, the contribution of non-copepod groups to total zooplankton abundance and biomass can be high (Wold et al. 2023), which was also the case in our study. Therefore, boreal species on the one hand can seasonally contribute to local zooplankton secondary production in Barents Sea and on the other hand can impact copepod secondary production through increased predation. Specific mortality rates of *Calanus* spp. residing in the surface layers in the Atlantic region in summer were estimated at  $-0.35 \text{ d}^{-1}$  and resulted from high predation pressure by hydrozoans and chaetognaths, increased natural mortality and high migration of *Calanus* spp. to deeper water layers (Basedow et al. 2014). In shallower, ice-free habitats, visually foraging fish can exert a significant predation pressure on copepods. As a result, abundance of large copepods is higher where sea-ice shades the water or the water column is deeper, allowing for an escape from visual predators through vertical migration (Langbehn et al. 2023). The pattern of lower copepod secondary production the Atlantic

Table 5. Secondary production estimates from other Arctic regions during comparable seasons. Production values of Dvoretzky & Dvoretzky (2009, 2012, 2024a,b) were recalculated from dry mass, according to their conversion factor: 1 mg dry mass = 0.4 mg carbon mass. Production values of Coyle & Pinchuk (2003) were recalculated from  $\text{mg C m}^{-2} \text{ d}^{-1}$  to  $\text{mg C m}^{-3} \text{ d}^{-1}$ , based on their sampling depth of 100 m. LOPC: laser optical plankton counter

Region	Season	Investigated mesozooplankton fraction	Production ( $\text{mg C m}^{-3} \text{ d}^{-1}$ )	Method	Source
Barents Sea, polar front	June	Total mesozooplankton	0.69	LOPC sampling and model D	This study
		Total copepods	2.80–3.65		
		Small copepods	0.00–2.93	Traditional net	
		Large copepods	0.32–1	sampling & model B	
Barents Sea, polar front	August	Total copepods	0.32–1	Hirst et al. (2003)	Dvoretzky & Dvoretzky (2024a)
NE Barents Sea	June–July	Total mesozooplankton	0.2–0.93	Hirst et al. (2003)	Dvoretzky & Dvoretzky (2024b)
S Barents Sea	July–August	Total copepods	0.04–0.44	Model B	Dvoretzky & Dvoretzky (2012)
SE Barents Sea	August	Total copepods	0.4–2	Model B	Dvoretzky & Dvoretzky (2009)
White Sea	June	Total copepods	~6.5	Physiological method	Primakov & Berger (2007)
Disko Bay, Greenland	June	Small copepods	0.08–0.16	Model A	Madsen et al. (2001, 2008)
Gulf of Alaska	June	Large copepods ( <i>Calanus</i> spp.)	0.5–2.2	Model B	Coyle & Pinchuk (2003)
		Total copepods	0.3–0.4		
Chukchi Sea	July	Planktonic crustaceans	0.4–4.1	Chitobiase method	Sastri et al. (2012)
Bering Sea	July	Small copepods	0.3–1.4	Combination of different growth rate equations	Kimmel et al. (2018)
		Large copepods	0.1–0.28		

region, observed in this study, can be explained by a combination of increased predation risk in the Atlantic region and higher food availability in other areas. At the time of our study, the microbial community was latitudinally structured and displayed a post-bloom state in the Atlantic region (Wiedmann et al. 2014), which probably promoted the growth of small copepods. Across the polar front, the community was in an earlier seasonal developmental state and still resembled a late bloom stage in the marginal ice zone in the Arctic region (Wiedmann et al. 2014), where reproduction of *Calanus* spp. was high. The interplay of the microbial food web and copepod secondary production is discussed in more detail in Section 4.3.

Another aspect that likely influenced the observed trends in copepod secondary production is the sampling design. Zooplankton distribution is very patchy and influenced by local eddies, meanders and biological cues (Sakshaug et al. 2009, Basedow et al. 2014, Trudnowska et al. 2016), which can result in the for-

mation of thin patches that can stretch horizontally over several kilometres (Trudnowska et al. 2016). Similar patches were observed in the present study through the use of the LOPC (size groups M and L, Fig. 4). When studying zooplankton trends with traditional net sampling, one of the main challenges is to achieve the appropriate spatial resolution, as patchiness can lead to high sampling variance. In addition to patchiness, net avoidance and extrusion of zooplankton and the estimation of filtered volume are aspects that add complexity to an accurate assessment of zooplankton trends (Runge & Roff 2000). Our sampling design consisted of a single vertical net haul at only 4 stations, raising the possibility that zooplankton patches might have been missed using the traditional net sampling approach. Because of the high contribution of mesozooplankton groups other than copepods in the Atlantic region (Fig. 6A,C,D,F), we likely excluded a large part of total mesozooplankton secondary production with the traditional

net sampling in this region, as we focused on copepods only. In the frontal and Arctic waters, however, other mesozooplankton groups were less abundant, and copepod secondary production therefore likely constituted most of the total mesozooplankton secondary production in these areas.

#### 4.2. Particle size distribution across the polar front inferred from LOPC sampling

The polar front is an important feature in structuring the distribution pattern of different mesozooplankton species. Secondary production of small mesozooplankton (size group S, 0.25–0.6 mm ESD) was high in the Atlantic region south of the polar front, while secondary production of medium- (M, 0.6–1.5 mm ESD) and large-sized mesozooplankton (L, 1.5–4 mm ESD) was patchily distributed across the study area and associated with areas of high chl *a* concentration (Fig. 5). These findings are consistent with the results of a previous LOPC study conducted at the polar front in the area of the West Spitzbergen Shelf (Trudnowska et al. 2016). Those authors found that small mesozooplankton, e.g. *Oithona* spp., *Triconia* spp., *Acartia* spp. and copepod nauplii, frequently accumulate in areas with density discontinuities, such as horizontal density gradients associated with the meeting of hydrographically different water masses (Trudnowska et al. 2016). The formation of a meltwater layer in the upper 20 m of the water column, present across the polar front at the time of our study, likely led to the development of a horizontal density gradient that facilitated the observed differences in the distribution of the small size group (Fig. 4). Patches of medium- and large-sized mesozooplankton, such as *Calanus* spp., were associated with areas of high chl *a* concentration (Fig. 4). This trend was also observed by Trudnowska et al. (2016) at the polar front and can likely be explained by the high food availability and active aggregation of grazers. During our study, most of the secondary production measured by the LOPC was located in the upper 50 m water column. Chl *a* is one of the factors included in the growth rate model of Zhou et al. (2010) that was used to estimate production, and the measured chl *a* concentrations were low at a depth deeper than 50 m. As a consequence, the secondary production values were low in this depth range. This might lead to an underestimation of the production of small-sized copepods, as their production is not limited by chl *a* availability (Hirst & Bunker 2003). Therefore, production estimates of size group S might be underesti-

mated to a depth of 100 m, where *Oithona similis*, the main representative of small-sized copepods in Arctic waters, is usually found (Lischka & Hagen 2005).

The LOPC counts all particles within a certain size range that are present in the water column and consequently includes not only zooplankton, but also other particles such as faecal pellets, marine snow and inorganic suspended material (Schultes & Lopes 2009). The contribution of such particles to total counts can be substantial, as observed during periods of high glacial runoff (Trudnowska et al. 2014) or high river runoff (Schultes & Lopes 2009). According to the indices developed by Espinasse et al. (2018), it can be said with high certainty that particles of size group S, observed in non-stratified AW during our study, were zooplankton, while an unknown fraction of aggregates contributed to LOPC counts in stratified waters of the polar front and the Arctic region. A simultaneous study by Wiedmann et al. (2014) found that the particulate organic carbon (POC) flux in Arctic waters was dominated by larger particles (0.5–2.8 mm ESD), which were most likely diatom aggregates and presumably contributed to the LOPC counts of size group S during our study. In Atlantic waters, a high POC flux of small particles (0.05–1.00 mm ESD) with a POC:volume ratio matching copepod faecal pellets was observed (Wiedmann et al. 2014). However, in all likelihood, these faecal pellets did not contribute to the small particles counted by the LOPC in the Atlantic region during our study, as they are fragile and therefore broken up by the MVP during towing.

#### 4.3. Copepod secondary production related to community composition inferred from WP-2 net and GoFlo bottle sampling

The variations in the contribution of different copepod communities to total copepod secondary production can be related to temperature and food availability across the polar front, as these factors are the key drivers of secondary production (Kiørboe & Sabatini 1995). Secondary production of large, broadcast-spawning copepods is primarily controlled by food availability, while the productivity of small, sac-spawning copepods is mainly controlled by temperature (Kiørboe & Sabatini 1995). Generally, developmental rates (time from egg to adult) of broadcast-spawning and egg-carrying copepods are the same, but broadcast spawners exhibit higher growth rates (increase in body weight over time), higher weight-specific fecundities (reproductive output relative to female body weight) and higher egg-production

rates (number of eggs produced per day) than egg-carrying copepods (Kiørboe & Sabatini 1995). Under non-limiting food conditions, the production of broadcast-spawning copepods can therefore be considerably higher than that of egg-carrying copepods (Kiørboe & Sabatini 1995). From our observations, we suggest that during a (late) phytoplankton bloom scenario in Arctic waters, *Calanus* spp. can outcompete small-sized copepods due to the high food availability and the low temperatures that restrict sac-spawner reproduction. In a post-bloom scenario in warm Atlantic waters, small-sized copepods play an important role in secondary production, as they profit from the warmer water temperatures (Barth-Jensen et al. 2020).

The Atlantic region (Stn M4) was in a nutrient-depleted post-bloom stage at the time of our study (Wiedmann et al. 2014), and a grazer community consisting mainly of small-sized egg-carrying copepod species and the large copepod *Calanus finmarchicus* was associated with the prevailing microbial food web (Franzè & Lavrentyev 2017). We observed high reproduction of *Oithona* spp. in Atlantic waters, which can be explained by the higher water temperatures of ca. 5°C in this region. Reproduction of *Oithona* spp. is positively correlated with increasing temperature, and potential hatching rates at the Atlantic station (M4) were at least 7 times higher than at the Arctic station (M1), when applying the hatching rate (HR) equation of Barth-Jensen et al. (2020) ( $HR = 0.018T + 0.013$ , assuming a temperature of 0°C at Stn M1 to avoid negative hatching rates). Small copepods live close to food saturation due to their size (Kiørboe & Sabatini 1995) and can consume a large range of prey, including ciliates, dinoflagellates, phytoplankton and faecal material (Gallienne & Robins 2001), which made their reproduction uncoupled from the phytoplankton bloom that was observed in Arctic waters. Productivity of large, broadcast-spawning copepods, e.g. *Calanus* spp., is mainly governed by food availability, and the effect is more pronounced on adult weight-specific fecundity than on juvenile growth (Kiørboe & Sabatini 1995). Assuming a gross growth efficiency (growth ingestion<sup>-1</sup>) of 0.3 for metazoan zooplankton (Ikeda & Motoda 1978), the ingestion rate of the *Calanus* spp. (CI–CVI) community can be assessed. In the Atlantic region (Stn M4), 7.8 mg C m<sup>-3</sup> d<sup>-1</sup> was needed to sustain *Calanus* spp. (CI–CVI) secondary production. No primary production was measured in this study, but chl *a* standing stock and microzooplankton production can indicate potential food limitation. Microzooplankton biomass was 5–8 times higher in the Atlantic region compared to the Arctic region and the polar front (Table S3; Franzè & Lavren-

tyev 2017). The estimated microzooplankton production in the Atlantic region was 17.7 mg C m<sup>-3</sup> d<sup>-1</sup> (Franzè & Lavrentyev 2017) and the chl *a* standing stock was 41 mg C m<sup>-3</sup> (C:chl *a* ratio = 50, Basedow et al. 2014). This relatively low standing stock might indicate that chl *a* was heavily grazed upon by the zooplankton community. The high secondary production of *C. finmarchicus* copepodites in the Atlantic region can likely be attributed to additional grazing on microzooplankton, as has previously been observed north of Svalbard (Svensen et al. 2019). *Calanus* spp. feed efficiently on diatoms but show a more varied diet outside of the spring bloom that can include a variety of proto- and microzooplankton (Cleary et al. 2017).

The polar front stations were characterized by a post-bloom phytoplankton community (Wiedmann et al. 2014). Low numbers of calanoid nauplii indicated that the mesozooplankton community was likely in a more mature state, meaning calanoid reproduction had already happened some weeks earlier. This is further affirmed by the presence of high numbers of young-stage calanoid copepodites, which are assumed to be the offspring of a late-spawning G<sub>0</sub> population (Arashkevich et al. 2002). The required food concentration to sustain *Calanus* spp. (CI–CVI) secondary production across the polar front was 6.9–9.8 mg C m<sup>-3</sup> d<sup>-1</sup>. Juvenile calanoid copepods achieve half their potential maximum growth at a chl *a* concentration of 0.6 mg m<sup>-3</sup>, which is one order of magnitude lower than the food concentration adults need (Hirst & Bunker 2003). Therefore, the observed low chl *a* standing stock of 0.55–0.9 mg m<sup>-3</sup> (27.5–45 mg C m<sup>-3</sup>) in combination with 1.7–2.3 mg C m<sup>-3</sup> d<sup>-1</sup> microzooplankton production might still be sufficient to fuel copepodite growth across the front.

The Arctic region (Stn M1) was in a late peak bloom stage, with loose drift-ice still present and a phytoplankton community mainly consisting of large diatom cells (mostly of the genera *Thalassiosira* and *Chaetoceros*) (Wiedmann et al. 2014). We observed a 'classical grazer food chain', typically linked to the phytoplankton spring bloom, where large-celled diatoms are consumed by copepods of the genus *Calanus*. The contribution of calanoid nauplii to the total copepod secondary production was highest in the Arctic region, indicating local reproduction of *Calanus*, most likely of *C. glacialis*, in response to the bloom. The required food concentration to sustain *Calanus* spp. (CI–CVI) secondary production in the Arctic region was 3.0 mg C m<sup>-3</sup> d<sup>-1</sup>. Naupliar stages I and II of both *C. finmarchicus* and *C. glacialis* do not feed (Breteler et al. 1982, Daase et al. 2011), and the

growth of the other naupliar stages is less strongly governed by food availability than adult fecundity is (Hirst & Bunker 2003). Therefore, the chl *a* standing stock of 98 mg C m<sup>-3</sup> and the estimated microzooplankton production of about 2 mg C m<sup>-3</sup> d<sup>-1</sup> (Franzè & Lavrentyev 2017) might be sufficient to fuel copepod secondary production in the Arctic region. Because copepod nauplii show on average 2 times faster developmental rates than copepodites (Kiørboe & Sabatini 1995), their contribution to overall secondary production can be substantial. Indeed, we observed that calanoid nauplii contributed 74% to total copepod secondary production in Arctic waters. To our knowledge, this study is one of the first to highlight the importance of nauplii for secondary production at the Barents Sea polar front.

## 5. CONCLUSIONS

The north-western Barents Sea is characterized by high secondary production during the summer, exceeding that of other Arctic regions. Contrary to the commonly held belief that oceanic fronts universally enhance secondary production, our observations present a more nuanced perspective for the Barents Sea polar front. While copepod secondary production was highest in the northern section of the polar front and in the Arctic region north of it, the total mesozooplankton secondary production was highest in the Atlantic region located to the south of the polar front. Two main factors influenced secondary production in the study region. Firstly, the advection of mesozooplankton biomass with the Norwegian Atlantic Current played a pivotal role. Through this process, boreal mesozooplankton locally contributed to the mesozooplankton secondary production in the Atlantic region and likely exerted significant predation pressure on large copepods, resulting in decreased copepod secondary production in this region. Secondly, the interplay between the sea-ice retreat, the meltwater front and the phytoplankton bloom status emerged as another important factor impacting secondary production. These complex interactions resulted in variations in water temperature and food availability across the polar front and particularly impacted copepod secondary production dynamics throughout the study region. In the Atlantic region, young developmental stages (CI–CIV) of *Calanus* spp. contributed most to copepod secondary production. This area also stood out as the only region where small-sized copepod species contributed noticeably to copepod secondary production, due to higher

water temperatures that favoured their reproduction. In the Arctic region, on the other hand, calanoid nauplii and older developmental stages (CV–CVI) contributed most to copepod secondary production. During the (late) phytoplankton bloom scenario that was observed in the Arctic region, *Calanus* spp. likely outcompeted small-sized copepods because of the high food availability and low water temperatures that restricted sac-spawner reproduction.

We demonstrate how estimates of copepod secondary production vary considerably with the chosen method to estimate copepod growth rates. However, the trends in the contribution of the different size classes to total copepod production were the same for all copepod growth rate models. During periods with high chl *a* concentrations, we recommend estimating copepod secondary production in the epipelagic layer of Arctic areas with the model of Hirst & Lampitt (1998), as it gives approximations of copepod growth rates at specific temperatures under food saturation. In periods with very low chl *a* concentrations, when large, predominantly herbivorous copepods are food limited, we recommend using a model that considers chl *a* as a food proxy, such as the model of Hirst & Bunker (2003). Secondary production of small copepods can be estimated year-round with the model of Hirst & Lampitt (1998), as growth of these copepods is more temperature- than food-limited. Combining high spatial- and taxonomic-resolution sampling using an optical plankton counter and traditional net sampling was a good approach to estimate secondary production across the Barents Sea polar front, and we recommend employing a combination of both sampling methods for future studies in high-latitude areas.

**Acknowledgements.** We thank the captain and the crew of RV 'Helmer Hanssen' for practical assistance during the fieldwork, and Katarzyna Dmoch for her analysis of the mesozooplankton samples. This work was part of the CONFLUX project, funded by Tromsø Forskningsstiftelse, and was additionally funded by the Research Council of Norway through the project 'The Nansen Legacy' (RCN # 276730).

## LITERATURE CITED

- Aarflot JM, Skjoldal HR, Dalpadado P, Skern-Mauritzen M (2018) Contribution of *Calanus* species to the mesozooplankton biomass in the Barents Sea. ICES J Mar Sci 75: 2342–2354
- Acha EM, Mianzan HW, Guerrero RA, Favero M, Bava J (2004) Marine fronts at the continental shelves of austral South America: physical and ecological processes. J Mar Syst 44:83–105

- Allen JT, Brown L, Sanders R, Moore CM and others (2005) Diatom carbon export enhanced by silicate upwelling in the northeast Atlantic. *Nature* 437:728–732
- Arashkevich E, Wassmann P, Pasternak A, Riser CW (2002) Seasonal and spatial changes in biomass, structure, and development progress of the zooplankton community in the Barents Sea. *J Mar Syst* 38:125–145
- Bakun A (1997) Patterns in the ocean: ocean processes and marine population dynamics. *Deep Sea Res B, Oceanogr Lit Rev* 5:530
- Barth-Jensen C, Koski M, Varpe Ø, Glad P, Wangensteen OS, Præbel K, Svensen C (2020) Temperature-dependent egg production and egg hatching rates of small egg-carrying and broadcast-spawning copepods *Oithona similis*, *Microsetella norvegica* and *Microcalanus pusillus*. *J Plankton Res* 42:564–580
- Basedow SL, Zhou M, Tande KS (2014) Secondary production at the polar front, Barents Sea, August 2007. *J Mar Syst* 130:147–159
- Basedow SL, Sundfjord A, von Appen WJ, Halvorsen E, Kwasniewski S, Reigstad M (2018) Seasonal variation in transport of zooplankton into the Arctic Basin through the Atlantic gateway, Fram Strait. *Front Mar Sci* 5:194
- Breteler WK, Fransz HG, Gonzalez SR (1982) Growth and development of four calanoid copepod species under experimental and natural conditions. *Neth J Sea Res* 16: 195–207
- Cleary AC, Søreide JE, Freese D, Niehoff B, Gabrielsen TM (2017) Feeding by *Calanus glacialis* in a high arctic fjord: potential seasonal importance of alternative prey. *ICES J Mar Sci* 74:1937–1946
- Conover RJ (1988) Comparative life histories in the genera *Calanus* and *Neocalanus* in high latitudes of the northern hemisphere. *Hydrobiologia* 167:127–142
- Coyle KO, Pinchuk AI (2003) Annual cycle of zooplankton abundance, biomass and production on the northern Gulf of Alaska shelf, October 1997 through October 2000. *Fish Oceanogr* 12:327–338
- Daase M, Søreide JE, Martynova D (2011) Effects of food quality on naupliar development in *Calanus glacialis* at subzero temperatures. *Mar Ecol Prog Ser* 429:111–124
- Derisio C, Alemany D, Acha EM, Mianzan H (2014) Influence of a tidal front on zooplankton abundance, assemblages and life histories in Peninsula Valdés, Argentina. *J Mar Syst* 139:475–482
- Dvoretsky VG, Dvoretsky AG (2009) Summer production of copepods in the Barents Sea. *Dokl Biol Sci* 428:451
- Dvoretsky VG, Dvoretsky AG (2012) Estimated copepod production rate and structure of mesozooplankton communities in the coastal Barents Sea during summer–autumn 2007. *Polar Biol* 35:1321–1342
- Dvoretsky VG, Dvoretsky AG (2024a) Marine copepod assemblages in the Arctic: the effect of frontal zones on biomass and productivity. *Mar Environ Res* 193:106250
- Dvoretsky VG, Dvoretsky AG (2024b) Local variability of Arctic mesozooplankton biomass and production: a case summer study. *Environ Res* 241:117416
- Erga SR, Ssebiyonga N, Hamre B, Frette Ø, Rey F, Drinkwater K (2014) Nutrients and phytoplankton biomass distribution and activity at the Barents Sea Polar Front during summer near Hopen and Storbanken. *J Mar Syst* 130:181–192
- Espinasse B, Basedow S, Schultes S, Zhou M, Berline L, Carlotto F (2018) Conditions for assessing zooplankton abundance with LOPC in coastal waters. *Prog Oceanogr* 163: 260–270
- Falk-Petersen S, Mayzaud P, Kattner G, Sargent JR (2009) Lipids and life strategy of Arctic *Calanus*. *Mar Biol Res* 5: 18–39
- Fer I, Drinkwater K (2014) Mixing in the Barents Sea Polar Front near Hopen in spring. *J Mar Syst* 130:206–218
- Forest A, Stemmann L, Picheral M, Burdorf L, Robert D, Fortier L, Babin M (2012) Size distribution of particles and zooplankton across the shelf-basin system in southeast Beaufort Sea: combined results from an Underwater Vision Profiler and vertical net tows. *Biogeosciences* 9: 1301–1320
- Fosshem M, Nilssen EM, Aschan M (2006) Fish assemblages in the Barents Sea. *Mar Biol Res* 2:260–269
- Franks PJS (1992) Phytoplankton blooms at fronts: patterns, scales, and physical forcing mechanisms. *Rev Aquat Sci* 6:121–137
- Franzè G, Lavrentyev PJ (2017) Microbial food web structure and dynamics across a natural temperature gradient in a productive polar shelf system. *Mar Ecol Prog Ser* 569: 89–102
- Gallienne CP, Robins DB (2001) Is *Oithona* the most important copepod in the world's oceans? *J Plankton Res* 23: 1421–1432
- Gawinski C, Dmoch K, Svensen C (2023) Mesozooplankton abundance, biomass and copepod secondary production at the Barents Sea polar front, June 2011. Sampling event dataset version 1.6. UiT The Arctic University of Norway, Tromsø
- Gawinski C, Daase M, Primicerio R, Amargant-Arumí M and others (2024) Response of the copepod community to interannual differences in sea-ice cover and water masses in the northern Barents Sea. *Front Mar Sci* 11:1308542
- Hassel A (1986) Seasonal changes in zooplankton composition in the Barents Sea, with special attention to *Calanus* spp. (Copepoda). *J Plankton Res* 8:329–339
- Herman AW, Beanlands B, Phillips EF (2004) The next generation of optical plankton counter: the laser-OPC. *J Plankton Res* 26:1135–1145
- Hirche HJ, Kosobokova K (2007) Distribution of *Calanus finmarchicus* in the northern North Atlantic and Arctic Ocean—expatriation and potential colonization. *Deep Sea Res II* 54:2729–2747
- Hirst AG, Bunker AJ (2003) Growth of marine planktonic copepods: global rates and patterns in relation to chlorophyll *a*, temperature, and body weight. *Limnol Oceanogr* 48:1988–2010
- Hirst AG, Lampitt RS (1998) Towards a global model of in situ weight-specific growth in marine planktonic copepods. *Mar Biol* 132:247–257
- Hirst AG, Roff JC, Lampitt RS (2003) A synthesis of growth rates in marine epipelagic invertebrate zooplankton. *Adv Mar Biol* 44:1–142
- Holm-Hansen O, Lorenzen CJ, Holmes RW, Strickland JDH (1965) Fluorometric determination of chlorophyll. *ICES J Mar Sci* 30:3–15
- Hunter MD, Price PW (1992) Playing chutes and ladders: heterogeneity and the relative roles of bottom-up and top-down forces in natural communities. *Ecology* 73: 724–732
- Huntley M, Boyd C (1984) Food-limited growth of marine zooplankton. *Am Nat* 124:455–478
- Huntley ME, Lopez MDG (1992) Temperature-dependent

- production of marine copepods: a global synthesis. *Am Nat* 140:201–242
- Ikeda TS, Motoda SI (1978) Estimated zooplankton production and their ammonia excretion in the Kuroshio and adjacent seas. *Fish Bull* 76:357–367
- Kimmel DG, Eisner LB, Wilson MT, Duffy-Anderson JT (2018) Copepod dynamics across warm and cold periods in the eastern Bering Sea: implications for walleye pollock (*Gadus chalcogrammus*) and the Oscillating Control Hypothesis. *Fish Oceanogr* 27:143–158
- Kiørboe T, Sabatini M (1995) Scaling of fecundity, growth and development in marine planktonic copepods. *Mar Ecol Prog Ser* 120:285–298
- Kwasniewski S, Hop H, Falk-Petersen S, Pedersen G (2003) Distribution of *Calanus* species in Kongsfjorden, a glacial fjord in Svalbard. *J Plankton Res* 25:1–20
- Langbehn TJ, Aarflot JM, Freer JJ, Varpe Ø (2023) Visual predation risk and spatial distributions of large Arctic copepods along gradients of sea ice and bottom depth. *Limnol Oceanogr* 68:1388–1405
- Le Feuvre J (1987) Aspects of the biology of frontal systems. *Adv Mar Biol* 23:163–299
- Lischka S, Hagen W (2005) Life histories of the copepods *Pseudocalanus minutus*, *P. acuspes* (Calanoida) and *Oithona similis* (Cyclopoida) in the Arctic Kongsfjorden (Svalbard). *Polar Biol* 28:910–921
- Liu H, Hopcroft RR (2006a) Growth and development of *Metridia pacifica* (Copepoda: Calanoida) in the northern Gulf of Alaska. *J Plankton Res* 28:769–781
- Liu H, Hopcroft RR (2006b) Growth and development of *Neocalanus flemingeri/plumchrus* in the northern Gulf of Alaska: validation of the artificial-cohort method in cold waters. *J Plankton Res* 28:87–101
- Liu GM, Sun S, Wang H, Zhang Y, Yang B, Ji P (2003) Abundance of *Calanus sinicus* across the tidal front in the Yellow Sea, China. *Fish Oceanogr* 12:291–298
- Loeng H (1991) Features of the physical oceanographic conditions of the Barents Sea. *Polar Res* 10:5–18
- Madsen SD, Nielsen TG, Hansen BW (2001) Annual population development and production by *Calanus finmarchicus*, *C. glacialis* and *C. hyperboreus* in Disko Bay, western Greenland. *Mar Biol* 139:75–83
- Madsen SD, Nielsen TG, Hansen BW (2008) Annual population development and production by small copepods in Disko Bay, western Greenland. *Mar Biol* 155:63–77
- Melle W, Skjoldal HR (1998) Reproduction and development of *Calanus finmarchicus*, *C. glacialis* and *C. hyperboreus* in the Barents Sea. *Mar Ecol Prog Ser* 169:211–228
- Munk P, Fox CJ, Bolle LJ, van Damme CJG, Fossum P, Kraus G (2009) Spawning of North Sea fishes linked to hydrographic features. *Fish Oceanogr* 18:458–469
- Owrid G, Soccal G, Civitarese G, Luchetta A and others (2000) Spatial variability of phytoplankton, nutrients and new production estimates in the waters around Svalbard. *Polar Res* 19:155–171
- Pedersen T, Mikkelsen N, Lindstrøm U, Renaud PE and others (2021) Overexploitation, recovery, and warming of the Barents Sea ecosystem during 1950–2013. *Front Mar Sci* 8:732637
- Primakov IM, Berger VY (2007) Production of planktonic crustaceans in the White Sea. *Russ J Mar Biol* 33: 305–310
- Reigstad M, Carroll J, Slagstad D, Ellingsen I, Wassmann P (2011) Intra-regional comparison of productivity, carbon flux and ecosystem composition within the northern Barents Sea. *Prog Oceanogr* 90:33–46
- Roura Á, Strugnell JM, Guerra Á, González ÁF, Richardson AJ (2018) Small copepods could channel missing carbon through metazoan predation. *Ecol Evol* 8:10868–10878
- Runge JA, Roff JC (2000) The measurement of growth and reproductive rates. In: Harris RP, Wiebe P, Lenz J, Skjoldal HR, Huntley M (eds) ICES zooplankton methodology manual. Elsevier, Academic Press, p 401–454
- Sakshaug E, Johnsen GH, Kovacs KM (eds) (2009) Ecosystem Barents Sea. Tapir Academic Press, Trondheim
- Sastri AR, Nelson RJ, Varela DE, Young KV, Wrohan I, Williams WJ (2012) Variation of chitobiase-based estimates of crustacean zooplankton production rates in high latitude waters. *J Exp Mar Biol Ecol* 414:54–61
- Schlutes S, Lopes RM (2009) Laser optical plankton counter and Zooscan intercomparison in tropical and subtropical marine ecosystems. *Limnol Oceanogr Methods* 7:771–784
- Silvert W, Platt T (1978) Energy flux in the pelagic ecosystem: a time-dependent equation. *Limnol Oceanogr* 23: 813–816
- Slagstad D, Tande KS (2007) Structure and resilience of overwintering habitats of *Calanus finmarchicus* in the Eastern Norwegian Sea. *Deep Sea Res II* 54:2702–2715
- Svensen C, Seuthe L, Vasilyeva Y, Pasternak A, Hansen E (2011) Zooplankton distribution across Fram Strait in autumn: Are small copepods and protozooplankton important? *Prog Oceanogr* 91:534–544
- Svensen C, Halvorsen E, Vernet M, Franzè G, Dmoch K, Lavrentyev PJ, Kwasniewski S (2019) Zooplankton communities associated with new and regenerated primary production in the Atlantic inflow north of Svalbard. *Front Mar Sci* 6:293
- Tande KS (1991) *Calanus* in North Norwegian fjords and in the Barents Sea. *Polar Res* 10:389–408
- Thornhill DJ, Mahon AR, Norenburg JL, Halanych KM (2008) Open-ocean barriers to dispersal: a test case with the Antarctic Polar Front and the ribbon worm *Parborlasia corrugatus* (Nemertea: Lineidae). *Mol Ecol* 17: 5104–5117
- Trudnowska E, Basedow SL, Blachowiak-Samolyk K (2014) Mid-summer mesozooplankton biomass, its size distribution, and estimated production within a glacial Arctic fjord (Hornsund, Svalbard). *J Mar Syst* 137:55–66
- Trudnowska E, Gluchowska M, Beszczynska-Möller A, Blachowiak-Samolyk K, Kwasniewski S (2016) Plankton patchiness in the Polar Front region of the West Spitsbergen Shelf. *Mar Ecol Prog Ser* 560:1–18
- Turner JT (2004) The importance of small planktonic copepods and their roles in pelagic marine food webs. *Zool Stud* 43:255–266
- Unstad KH, Tande KS (1991) Depth distribution of *Calanus finmarchicus* and *C. glacialis* in relation to environmental conditions in the Barents Sea. *Polar Res* 10:409–420
- Våge S, Basedow SL, Tande KS, Zhou M (2014) Physical structure of the Barents Sea Polar Front near Storbanken in August 2007. *J Mar Syst* 130:256–262
- Wassmann P, Ratkova T, Andreassen I, Vernet M, Pedersen G, Rey F (1999) Spring bloom development in the marginal ice zone and the central Barents Sea. *Mar Ecol* 20: 321–346
- Wassmann P, Reigstad M, Haug T, Rudels B and others (2006) Food webs and carbon flux in the Barents Sea. *Prog Oceanogr* 71:232–287

- Wiedmann I, Reigstad M, Sundfjord A, Basedow S (2014) Potential drivers of sinking particle's [sic] size spectra and vertical flux of particulate organic carbon (POC): turbulence, phytoplankton, and zooplankton. *J Geophys Res Oceans* 119:6900–6917
- Wolanski E, Hamner WM (1988) Topographically controlled fronts in the ocean and their biological influence. *Science* 241:177–181
- Wold A, Hop H, Svensen C, Søreide JE, Assmann KM, Ormanczyk M, Kwasniewski S (2023) Atlantification influences zooplankton communities seasonally in the northern Barents Sea and Arctic Ocean. *Prog Oceanogr* 219:103133
- Zamora-Terol S, Nielsen TG, Saiz E (2013) Plankton community structure and role of *Oithona similis* on the western coast of Greenland during the winter–spring transition. *Mar Ecol Prog Ser* 483:85–102
- Zhou M (2006) What determines the slope of a plankton biomass spectrum? *J Plankton Res* 28:437–448
- Zhou M, Carlotti F, Zhu Y (2010) A size-spectrum zooplankton closure model for ecosystem modelling. *J Plankton Res* 32:1147–1165

*Editorial responsibility:* Deborah K. Steinberg,  
Gloucester Point, Virginia, USA  
*Reviewed by:* A. Cornils and 2 anonymous referees

*Submitted:* July 2, 2023

*Accepted:* March 11, 2024

*Proofs received from author(s):* April 26, 2024